1 Introduction

1.1 Silicon and the semiconductor industry

Silicon has been ruling the semiconductor industry unarguably for the last few decades. It is a semiconductor, meaning that it has a small band gap (1.1 eV), that is tunable via doping with other elements. Conductivity of a semiconductor like silicon can be easily switched on or off by a magnetic or an electric field, change in temperature, or even by mechanical deformation. This is essential for the function of transistors or sensing devices. However, there are other elements and compounds which also possess these qualities and are used in the semiconductor industry. But, silicon indisputably is the most popular choice due to its low cost from high abundance in our Earth's crust, and having its own natural oxide, i.e., SiO_2. It has relatively good temperature range, and suitable for high frequency operations unlike the more sensitive germanium. Moreover, the fact that the reverse saturation current of silicon is in the order of nanoamperes as compared to that of germanium which is in the order of microamperes, overrides the undesirable fact that silicon has greater barrier potential (0.7 V) as compared to germanium (0.3 V).

In 1965, Gordon Moore, co founder of Intel, stated that the density of transistors per square inch on the integrated circuits had doubled up every one and a half years since the integrated circuit was invented. He thus predicted that this trend would surely continue for the foreseeable future. Half a century after this golden observation, VLSI has hit a brick wall. The incessant demand for increasing high power and decreasing chip size has forced the semiconductor industry to reach new limits in fabrication. So far the smallest commercially available transistors using silicon and the other traditional semiconductors has been made by Intel having a size of 14 nm. However, it is hazy how the semiconductor industry can keep scaling down the traditional transistors much further or what might replace them. As the transistors get smaller and smaller, more issues like chip overheating , short channel effects and defect densities etc. become harder to hold back. Current transistor sizes are in the order of a few atoms. The smallest production technology in terms of the size of current transistors is 14 nanometers. Silicon is 0.222 nm in diameter. So the smallest

commercially available silicon transistors are even less than the thickness of 100 silicon atoms. Soon we are to hit the physical barriers of atoms. In order to keep up with the Moore's Law, right now the industry has to scale down to 5 nm. An immediate answer to this catastrophic situation lies with nanotechnology. Nanotechnology deals with materials in nanoscale whose properties can be tailored as per design parameters as compared to the characteristic properties of their bulk counterparts. It hints at to switch over from silicon to a variety of alternative materials with better electronic properties at smaller size scales in order to continue the journey of the semiconductor industry smoothly to the future. Thus the search for such materials is on full swing.

1.2 2D Materials: Alternative to Silicon

The limits of further miniaturization of silicon nanoelectronic devices lead to an emerging development of novel nanomaterials. Electronic materials, such as semiconductor nanowires, carbon nanotubes, III-V compound semiconductors,are proposed as promising candidates to replace silicon in electronic devices. On the other side, two-dimensional materials, like graphene and the transition-metal chalcogenides, are attractive for the novel nanoelectronic devices because, compared to working with one dimensional materials, obviously, it is relatively easy to tailor them in the desired shape and fabricate very complex structures out of them. Being just a few angstroms thick, the 2D materials are very attractive for new generation transistors. The successful isolation of 2D graphene from graphite has led to its extensive study in physics, materials, and nanoengineering due to its extraordinary electrical and mechanical properties.

Thus, graphene is a strong contender as a 2D device material. It has high electron mobility and room temperature, thermal conductivity and excellent optical transmittance. It is chemically inert and has a large Young's modulus[1]. All these qualities are highly sought after in any semiconducting material. However, its lack of band gap and its semi-metal behaviour rules it out as a semiconductor. Band gap engineering is a prime necessity for graphene to have a band gap, However that in turn affects its desirable qualities in an inverse fashion.

The search for 2D materials has hence widened its radius to encompass other materials that exhibit properties similar to that of traditional semiconductors and graphene. Transition metal dichalcogenide crystal monolayers can probably be an alternative to silicon. They are

structurally stable and exbihit electron mobilities comparable to those of silicon, so that they can be used for fabrication of transistors. Transition metal dichalcogenide (TMDC) monolayers are atomically thin semiconductors of the type MX_2, with M a transition metal atom (Mo, W, etc.) and X a chalcogen atom (S, Se, or Te.). One layer of M atoms is sandwiched between two layers of X atoms. TMDCs have layered structures similar to that of graphene, are inexpensive due to their abundance and have large band gaps[37]. Semiconductors are typically efficient emitters if their band gap is direct. Owing to their direct band gap which lies in the visible range (between 400 nm and 700 nm), TMDC monolayers are promising materials for optoelectronics applications. On the other hand, their bulk counterparts when reduced to the thickness of two monolayers still have an indirect band gap. Small thickness (one monolayer), high carrier mobility, direct band gap and high on/off ratio of TMDC devices are potentially interesting for a variety of applications.

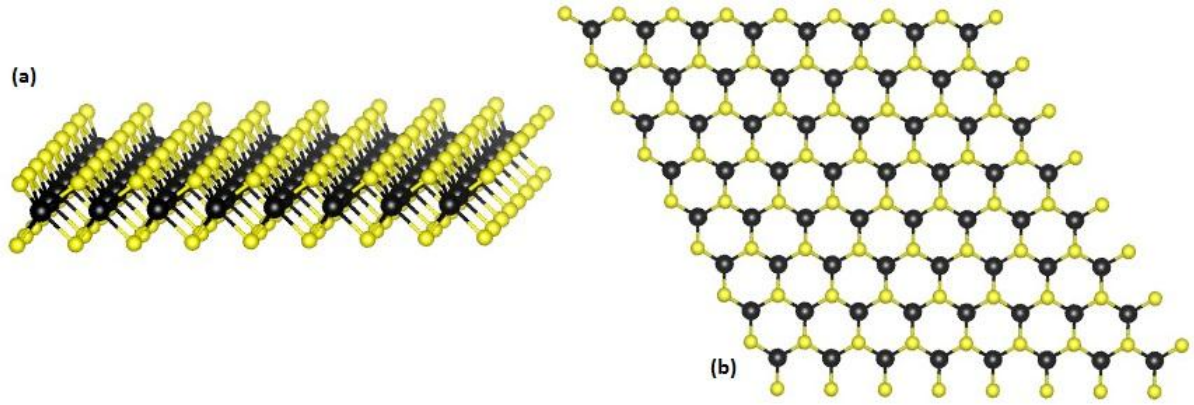

Figure 1.1(a) Structure of a hexagonal TMDC monolayer. M atoms are in black and X atoms are in yellow. (b) A hexagonal TMDC monolayer seen from above.

Another interesting 2D material is crystalline hexagonal boron nitride, which also possesses layers that are weakly held together by van der Waals forces. However, it has a very large band gap in the UV region and therefore has more insulating properties than TMDC, and has proven to be a superior substrate for graphene devices due to a lack of dangling bonds[40].

1.3 Objective

The path beyond 14 nm is undoubtedly treacherous, and by no means, is a sure thing. With each step down, the scaling process becomes more and more complex, and thereby, more expensive and more likely to be plagued by low yields. Most probably, there may be better gains that may be achieved from moving off- track, towards architectures and materials which can operate with more parallelism and at faster frequencies , rather than brute-forcing

the continuation of the age- old Moore's law. Thus, the focus of this project is to implement a relatively inexpensive method of controllable growth of TMDC monolayer, which may be feasible to be used for device fabrication. The as- produced samples are to go through certain standard characterization techniques in order to ascertain their quality. If the synthesized samples match with the expected morphology and properties of the material chosen, then further work would be carried out for the commercialization of the method. This could pave the way to flexible and transparent high performance electronics.

Molybdenum disulphide is chosen because of its desirable traits for use as a 2D semiconductor. MoS_2 as well as its pre-fabrication forms such as MoO_3 are relatively inexpensive and abundant[2] compared to selenium or tungsten. It is also known to be one of the more stable layered transition metal dichalcogens[3]. Its large direct band gap of 1.8 eV also makes it useful in optoelectronic applications like, light detectors, emitters and solar cells[9].

2 Characteristics of Molybdenum Disulphide

2.1 Bulk MoS_2

Molybdenum is a Period 5, Block D element, and sulfur is a Period 3, Block P element. Molybdenum disulfide is the inorganic compound with the formula MoS_2. Bulk MoS_2 is a shiny black solid having qualities quite similar to those of graphite. It has a layered structure where the layers are weakly bound by van der Waals forces. It is commonly found in a hexagonal 2H-MoS_2 stacking alignment. But it can also be found in a rhombohedral 3R-MoS_2 structure. This structure easily decomposes to its more stable hexagonal counterpart upon heating. It is relatively inexpensive and is easily formed by sulphurization of molybdenum trioxide or molybdenum metal. The other methods of growth would be expounded on in detail in chapter 5.

Figure 2.1 Molybdenite

2.1.1 Properties

Physical Properties: In MoS_2, each Mo (IV) center occupies a trigonal prismatic coordination sphere that is bound to six sulfide ligands. Each sulfur centre is pyramidal and is connected to three numbers of Mo centres. These trigonal prisms are interconnected in such a way so as to give a layered structure, where the molybdenum atoms are sandwiched between the layers of sulfur atoms. Because of the weak van der Waals interactions between the sheets of sulfide atoms, MoS_2 has low coefficient of friction, resulting in its lubricating properties.

Chemical Properties: Molybdenum disulfide is stable in air and attacked by only

aggressive reagents. It is insoluble in water and dilute acids. It reacts with oxygen upon heating forming molybdenum trioxide:

$$2\ MoS_2 + 9\ O_2 \rightarrow 2\ MoO_3 + 4\ SO_3$$

Chlorine attacks MoS_2 at elevated temperatures to form molybdenum pentachloride:

$$2\ MoS_2 + 7\ Cl_2 \rightarrow 2\ MoCl_5 + 2\ S_2Cl_2$$

2.1.2 Applications

Lubricant: MoS_2 with particle sizes in the range of 1–100 μm is a common dry lubricant confering high lubricity and stability at up to 350°C in oxidizing environment. The sliding friction tests of MoS_2 using one pin on disc tester at low loads (0.1–2 N) give friction coefficient values of < 0.1.

Petroleum Refining: MoS_2 is employed as a cocatalyst for desulfurization in petrochemistry.

Improved Composites: When added to plastics, the MoS_2 forms a composite which has improved strength as well as reduced friction. Polymers that are filled with MoS_2 include Teflon, nylon, and Vespel. The self-lubricating composite coatings used for high-temperature applications have been developed consisting of molybdenum disulfide.

2.2 Monolayer MoS_2

Molybdenum disulfide nanoparticles possess good catalytic activity, a low friction coefficient and excellent physical properties. They also have high reactivity, a large active surface area and also, increased adsorption capacity compared to the bulk material. Much research is focused on generating unusual morphologies of MoS_2. Multilayer sheets as well as nanotubes and buckyball-like molecules composed of MoS_2 are produced which exhibit unusual tribological and electronic properties. The distinguishing properties of MoS_2 monolayer namely its crystal structure, band gap and electron mobility, as compared to its bulk counterpart are briefly summarized below:

2.2.1 Band Gap

It has been found experimentally that monolayer MoS_2 has a large direct band gap of 1.8 eV.

This is much larger than that of its bulk form which is indirect band gap of 1.29 eV[2]. This enables the MoS_2 monolayer to possess a tunable band gap which is based on the number of layers that has been grown. In fact, MoS_2 may also have a band gap which can be tuned by means of an external electric field, as reported by *A. RamasubRamaniam et al.* [23] with calculations.

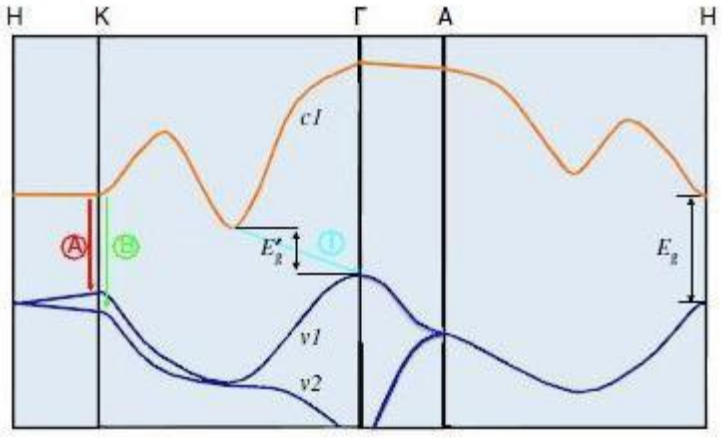

Figure 2.2 Band structure of bulk MoS_2, where A and B depict the direct gap transitions, as opposed to the indirect gap transition shown by I.[2]

2.2.2 Crystal Structure and Shape

Much of the desired qualities of molybdenum disulphide may be due to its crystal structure in its monolayer form. MoS_2 has a hexagonal structure consisting of S-Mo-S layers. This sandwich structure that it possesses accounts for its ability to be grown layer upon layer. An atomic plane of Mo atoms is found in this sandwich structure between two layers of S atoms in a trigonal prismatic structure, as shown in Figure 2.2 below[3].

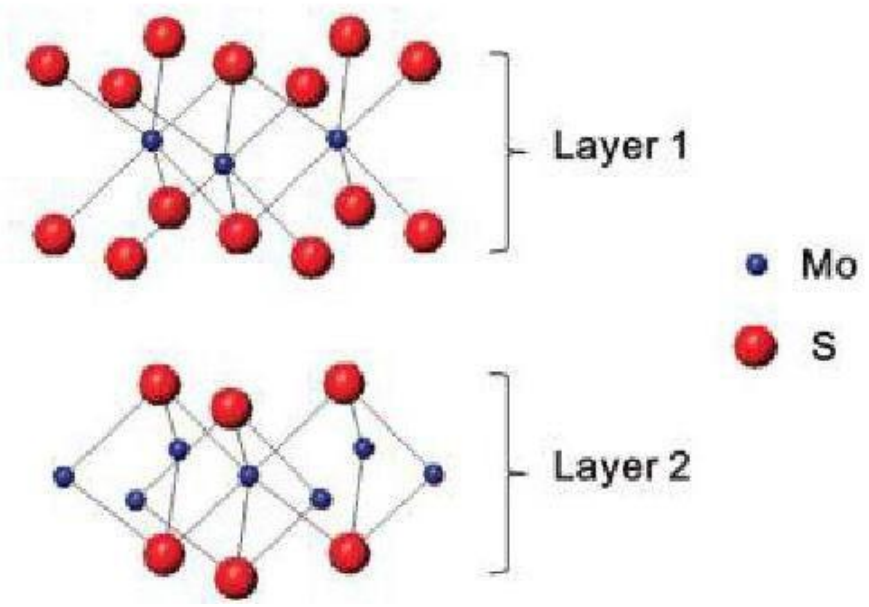

Figure 2.3 Bilayer structure of MoS_2.[3]

Each molybdenum atom is bound to six sulphur atoms in this trigonal prismatic fashion while each sulphur atom is connected to three molybdenum atoms in a pyramidal structure. Since the adjacent sheets of sulphur atoms only have weak van der Waals forces acting between them, they can be cleaved or separated easily from each other using a micromechanical cleavage technique[5].

MoS_2 is also found to be relatively stiff and is resistant to breakage, allowing for potential applications in flexible electronics[8].

Monocrystalline MoS_2 has been found to take on an interesting triangle shaped structure when it is grown. It is usually observed to takes on either a Mo-zigzag edge or S-zigzag edge[4]. A bright field image of an Mo-zigzag edge MoS_2 triangle is shown in Figure 2.4.

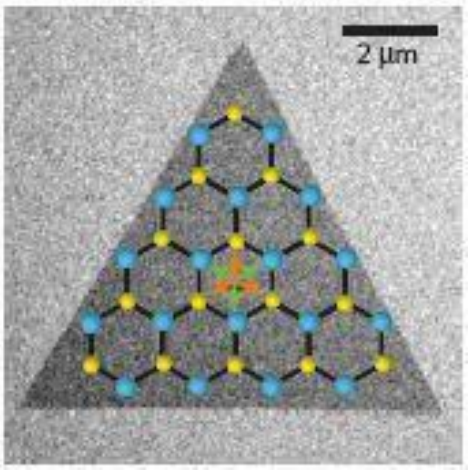

Figure 2.4 Bright field image of an MoS_2 crystal.[4]

2.2.3 Electronic and Optical Properties

MoS_2 monolayer can transmit very high current densities close to 5 x 10^7 A/cm^2, even higher than that of copper[6]. This is plotted in Figure 2.4, which shows the maximum attainable current in a monolayer MoS_2 device having channel width 2µm and length 500 nm.

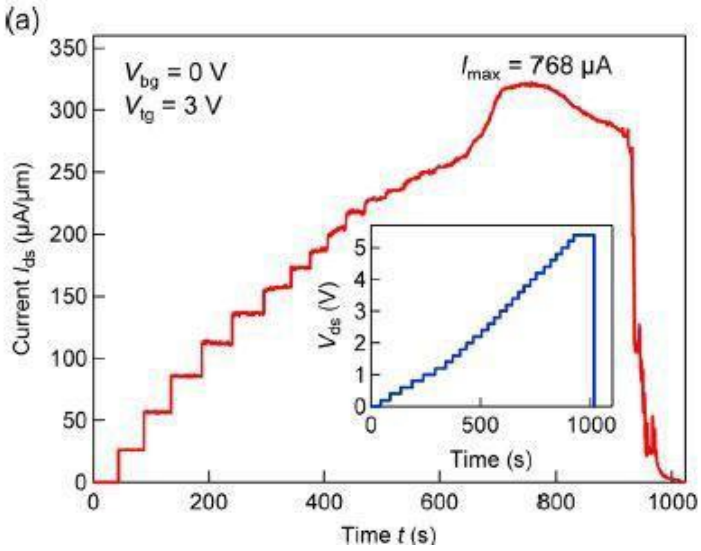

Figure 2.5 Time trace of drain current through a monolayer MoS_2 channel. The inset shows the time trace of the drain voltage.[6]

MoS_2 also has a high on/off ratio of 10^8, which aids in preventing leakages and power loss. It has been found that MoS_2 has electron mobility similar to silicon[7].

MoS_2 exhibits strong fluorescence due to its direct band gap. Coupled with its tunable band gap, MoS_2 is a strong contender in optical sensing or emitting devices operating at different optical frequencies and wavelengths.

2.2.4 Mechanical Properties

MoS_2 also exhibit excellent mechanical properties, making it ideal for nanodevice manufacturing. *Bertolazzi et al.* striked a comparison of strength and elasticity of MoS_2 with that of steel and found it to be comparable[8]. This group also reports that MoS_2 has an elasticity comparable with polymer thin films like polydimethylsiloxane and polyimide used in flexible electronics currently, and can be integrated with them theoretically.

3 Literature survey

A literature survey forms an important and indispensable module of a research project. It throws light on the amount of study done so far in the chosen subject matter, showcases the flaws and gaps in the previous research, pinpoints the new scopes of research arising out of those studies, highlights the status of research being carried out by the contemporary research groups in the relevant field around the globe and finally, saves time, funds and energy of a researcher from ending up in some conclusions which have already been found out by some other research group at some early date. Also, it prevents the research knowledge base from being plagued by plagiarism to a great extent.

A substantial amount of literature review has been done in this project. This chapter provides a summary on the different synthesis methods for the growth of large area monolayer MoS_2, adopted by different research groups and their pros and cons as well as their feasibility in commercialization. Moreover, it throws light on the study carried out around the globe on the properties and ways and means to tailor them as per the needs of the semiconductor industry.

Title: Synthesis of Large-Area MoS_2 Atomic Layers with Chemical Vapor Deposition.

Experimental Conditions: Lee et al.[14] conducted this experiment in three different ways, using three seeding agents, namely, reduced graphene oxide (rGO), PTCDA or PTAS, one at a time. SiO_2/Si substrate was faced down and mounted on the top of a ceramic boat containing MoO_3 powder (0.4 g). Another ceramic boat containing sulfur powder (0.8 g) was placed adjacent to the MoO_3 powder. Prior to the dersired growth, a small droplet of aqueous reduced graphene oxide (rGO), PTCDA or PTAS solution, was spin coated on the substrate surface which was followed by drying at 50℃. During this synthesis of MoS_2 sheets, reaction chamber was heated upto 650℃ in a stable nitrogen environment. At such an elevated temperature, the MoO_3 powder reacted with the sulfur vapour to grow MoS_2 films.

Characterisation Results:

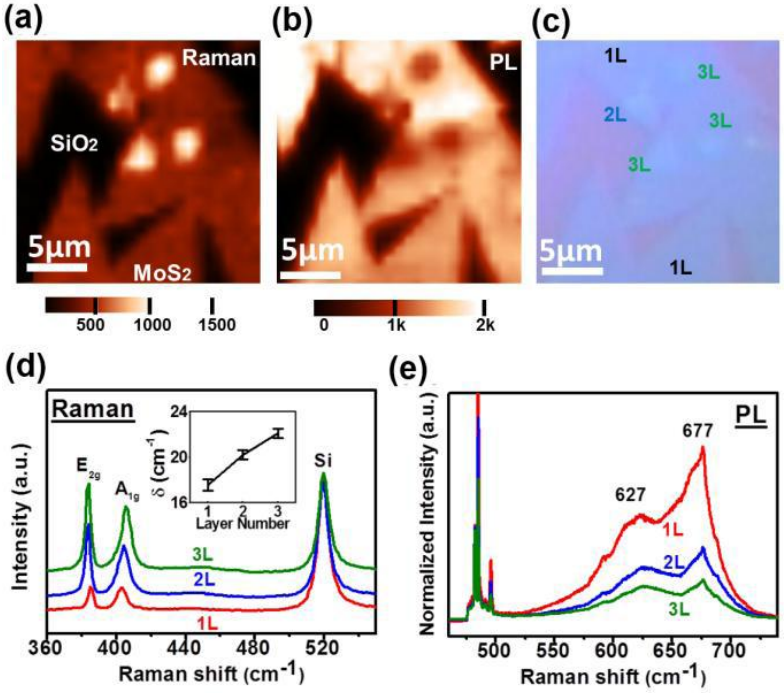

Figure 3-1(a) Raman peak intensity mapping (360 ~ 420 cm-1), (b) PL peak intensity mapping (650 ~ 700 nm) and (c) OM image of the selected area with various MoS_2 layer thickness (1L, 2L and 3L). (d) Raman spectra and (e) photoluminescence of the monolayer, bilayer [14]

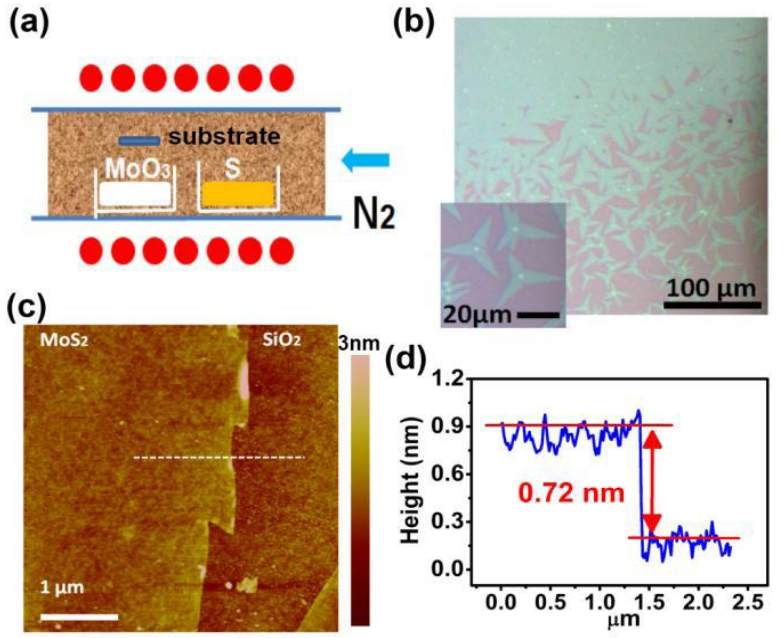

Figure 3-2(a) Schematic experimental set-up. (b) The OM of the MoS_2 layers grown pretreated with rGO solution. (c) AFM image of a monolayer MoS_2 film(d) The thickness of the MoS_2 layer from the AFM cross-sectional profile along the line indicated in (c).[14]

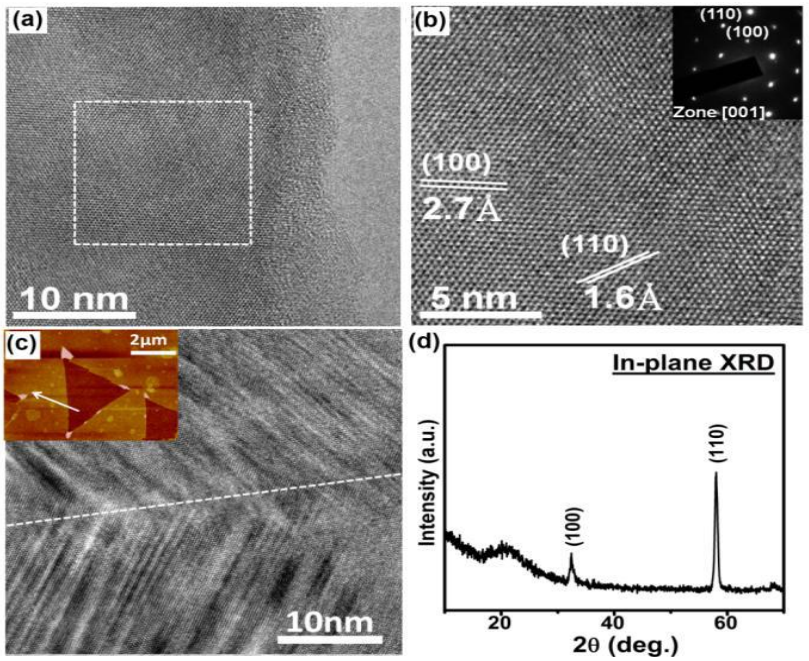

Figure 3-3(a)TEM image of MoS_2 monolayer.(b)HR-TEM image of the marked area in figure (a) with an inset showing SAED pattern.(c)TEM image for the MoS_2 domain boundary at the location as indicated by the inset AFM image.(d)In-plane XRD result for MoS_2 monolayer[14]

Conclusions : TEM and SAED demonstrate the exhibition of six-fold symmetry hexagonal lattice as well as high crystallinity by the monolayer of MoS_2.

Thickness of the as- produced MoS_2 layer is 0.72 nm. as obtained from AFM characterization.

The MoS_2 monolayer sheet is found to exhibit two characteristic Raman bands at 403.8 and 385.8 cm^{-1} with full-width-half-maximum (FWHM) values 6.6 and 3.5 cm^{-1} respectively, corresponding to A_{1g} and E_{2g} modes. This peak frequency difference between the A_{1g} and E_{2g} modes (Δ) is useful in identification of the number of layers of MoS_2. The value of Δ (18 cm^{-1}) is an evidence of the existence of monolayer of MoS_2.

PL spectrum displays two pronounced emission peaks at 627 and 677 nm. and those emissions are termed as A1 and B1 direct excitonic transitions. Emission intensity (which is normalized by Raman scattering at ~482 nm) visibly decreases with the number of layers. This is due to the fact that the optical bandgap transforms from the indirect to the direct one when the dimension of MoS_2 is decreased from the bulk form to the monolayer sheet.

Title: Growth of Large-Area and Highly Crystalline MoS_2 Thin Layers on Insulating Substrates
Experimental Conditions: Keng-Ku Liu et al.[12] conducted thermolysis process for the synthesis of thin layered MoS_2 on the insulating substrates. Precursor $(NH_4)_2MoS_4$ is dip-

coated on sapphire or SiO_2/Si substrates that is followed by two-step annealing process.

0.25 g of high purity $(NH_4)_2MoS_4$ is added to 20 mL of dimethylformamide (DMF) in order to form the 1.25 wt % solution. This solution is sonicated for about 20 min prior to use. The insulating substrate (like, sapphire or 300 nm SiO_2 on Si (SiO_2/Si)) is first cleaned with standard piranha solution (H_2SO_4/ H_2O_2 ~ 7/3). After about 10 min. of baking on hot plate at approximately 80 °C, substrate is immersed into $(NH_4)_2MoS_4$ solution, which is followed by the slow pulling (0.5 mm/s) in order to form a thin $(NH_4)_2MoS_4$ film. Then the substrate is baked on hot plate at approximately 120 °C for about 30 min. The as-prepared thin $(NH_4)_2MoS_4$ film is placed in cold zone of quartz tube where a gas mixture (Ar/H_2 flow rate = 4/1; at 1 Torr). is flowing. When center of the furnace reaches 500 °C, substrate is moved to hot zone of furnace for first annealing process. This chamber is kept at low pressure (1 Torr) in inert Ar/H_2 atmosphere (flow rate 4:1) in order to efficiently remove NH_3 molecules, residual solvent and other byproducts that are dissociated from those precursors. After sixty minutes, the sample is moved to the cold zone, and the inert gas environment is switched to Ar (or Ar + S) at about 500 Torr. The sample is then moved to center of furnace again for second annealing process when the hot zone reached upto 1000 °C whereby annealing is performed in in the mixture of Ar and sulfur or pure Ar. Sulfur can be used as a protection gas against oxidation. The sulfur is introduced then into the chamber in a powdery form, and these powders get converted to sulfur vapours at process temperature.

Characterisation Results:

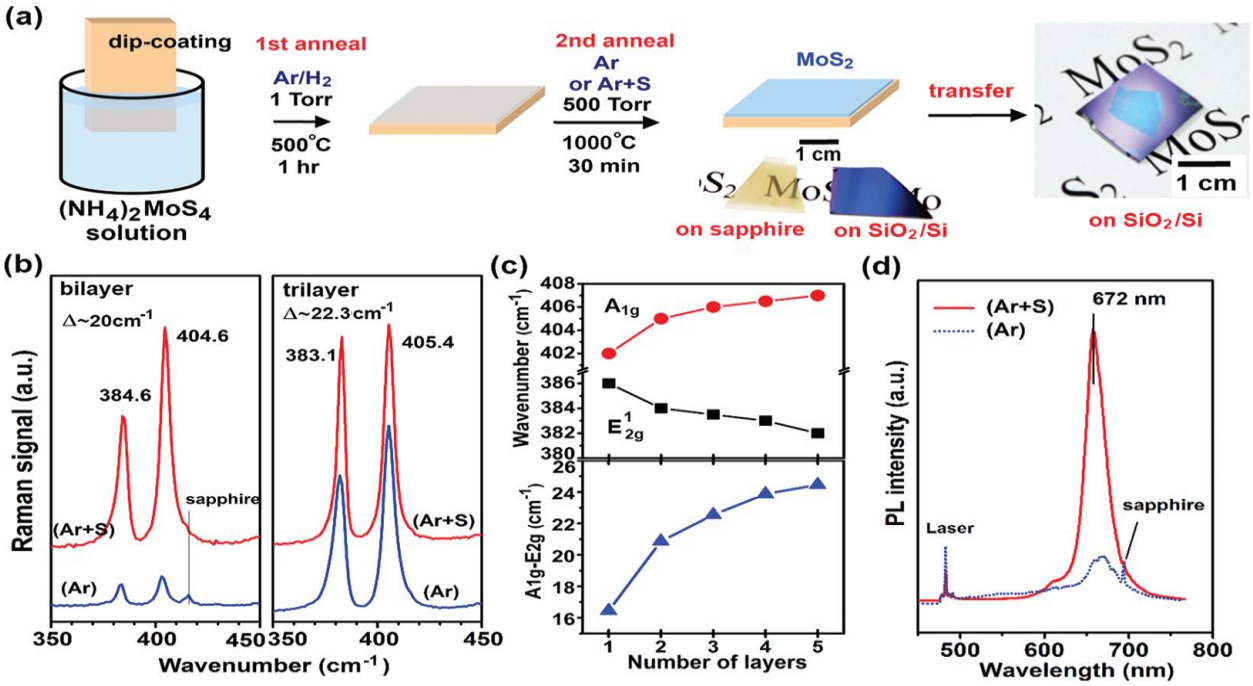

Figure 3-4. (a) Schematic illustration of the two-step thermolysis process for the synthesis of MoS_2 thin layers on insulating substrates. The precursor $(NH_4)_2MoS_4$ was dip-coated on SiO_2/Si or sapphire substrates followed by the two-step annealing process. The as-grown MoS_2 film can be transferred onto other arbitrary substrates. (b) Raman spectra for the bilayer and trilayer MoS_2 sheets grown on sapphire substrates (excitation laser: 473 nm), where the labels (Ar) and (Ar + S) represent the MoS_2 sheets separately prepared in pure Ar and in the mixture of Ar and sulfur during the second annealing. (c) Energies of the two characteristic Raman peaks for the micromechanically exfoliated MoS_2 films with various number of layers. The peak energy difference shown in the bottom graph can be used to identify the number of MoS_2 layers. (d) The PL intensity of the trilayer MoS_2 thin films prepared in (Ar + S) is stronger than those prepared in pure Ar (excitation laser 473 nm; spectra were normalized by Raman scattering peak at around 482 nm).[12]

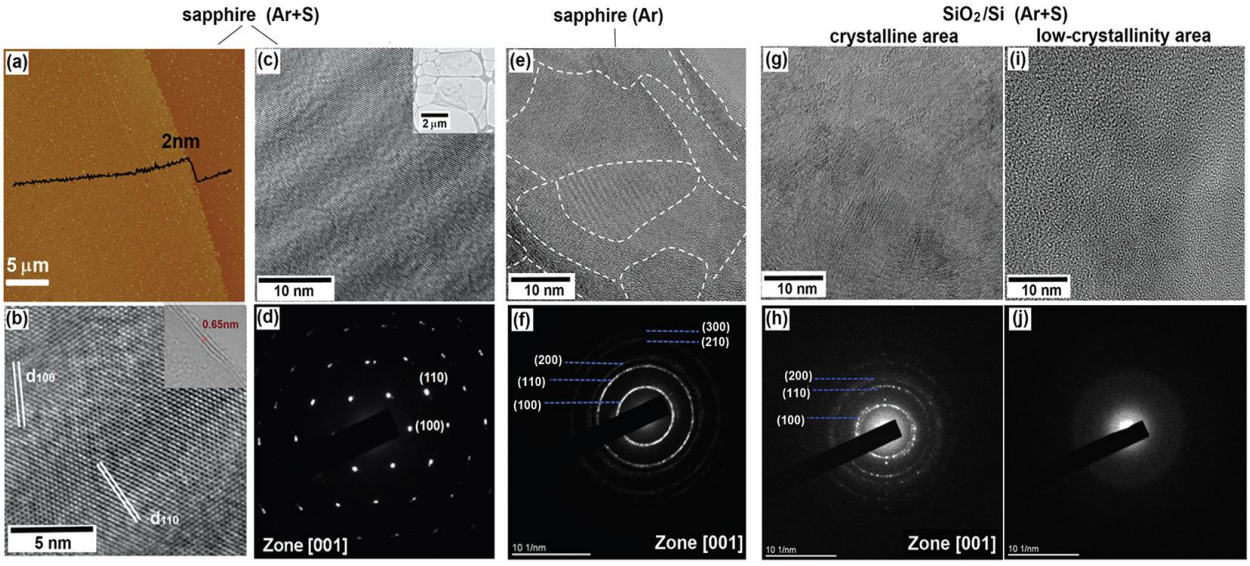

Figure 3-5. (a) AFM image of the MoS_2 trilayer grown on a sapphire substrate annealed with the presence of sulfur (Ar + S). (b) High-resolution TEM image for the MoS_2 trilayer. The d100 is 0.27 nm, and d110 is 0.16 nm. Inset is the TEM image of MoS_2 film edge, where three layers of MoS_2 are identified. (c) TEM image and (d) the SAED pattern of the MoS_2 trilayer sample discussed in (b). (e) TEM image and (f) the SAED pattern for the MoS_2 grown on sapphire with Ar annealing. (g, i) TEM images and (h, j) the SAED patterns for the MoS_2 trilayer grown on a SiO_2/Si substrate annealed with (Ar + S).[12]

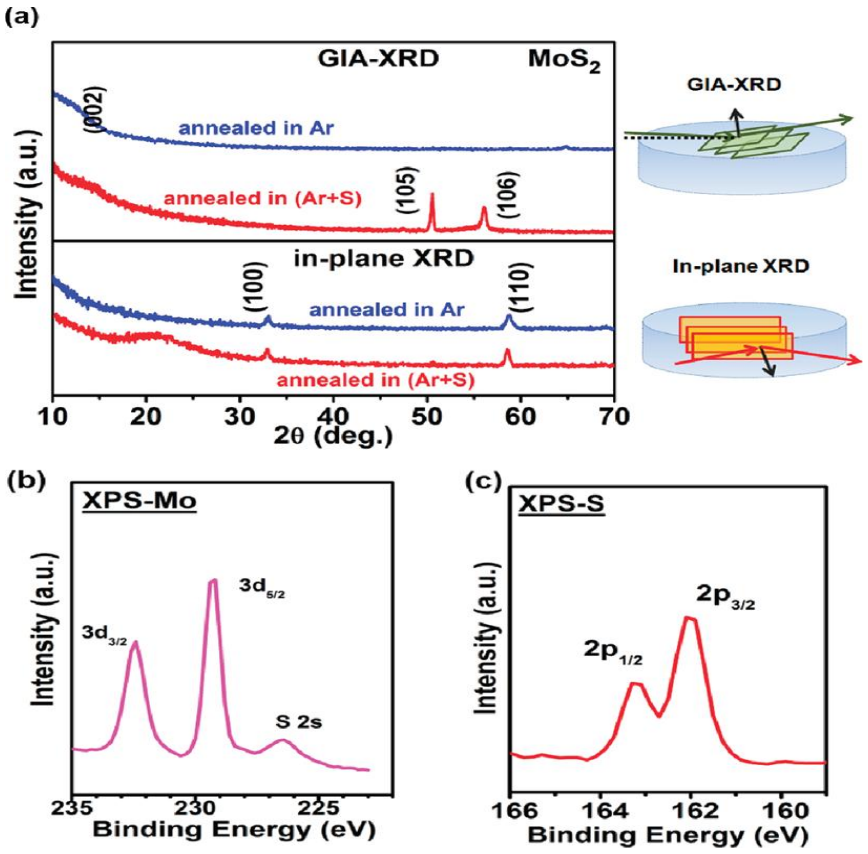

Figure 3-6. (a) Glancing incidence angle X-ray diffraction (GIA-XRD) and in-plane X-ray diffraction (in-plane XRD) patterns of the MoS_2 trilayers. (b, c) X-ray photoemission spectroscopy (XPS) measurements for the binding energies of Mo and S in the MoS_2 trilayers annealed with sulfur.[12]

Conclusions: This is the two-step thermolysis process used to synthesize the large-area as well as highly crystalline thin layered MoS_2. Addition of sulfur during the elevated-temperature annealing radically enhances the crystallinity of the MoS_2, as observed by various microscopic and spectroscopic characterizations including XRD ,Raman, PL, SAED and TEM.

Title: Synthesis of bilayer MoS_2 nanosheets by a facile hydrothermal method and their methyl orange adsorption capacity.

Experimental conditions: Lijuan Ye et al.[42] reported that ammonium molybdate ($(NH_4)_6Mo_7O_{24}$.$4H_2O$) alongwith elemental sulfur (S) powder are used as the molybdenum and sulfur sources, respectively. Firstly, $(NH_4)_6Mo_7O_{24}$.$4H_2O$ and S mixtures in various nominal mole ratios of the S to Mo are added to 100 mL beakers and then the 12 mL hydrazine monohydrate (N_2H_4 .H_2O, 85%) is used as the reducing agent and also, 20 mL distilled water are dropped into this mixture. After continual stirring for about 30 min, finally the mixture is transferred into a 50 mL Teflon-lined stainless steel autoclave and also, some extra distilled water is used in order to fill the autoclave upto 80% of total volume. The autoclave is then

tightly sealed and maintained about 180℃ in an air oven for a duration of 40 h. After cooling to the room temperature naturally, final reaction products are centrifuged as well as washed successively with diluted hydrochloric acid (HCl) ,distilled water and ethanol for multiple times. The black precipitates are then collected and dried in vacuum for 30 hr at 60℃.

Characterisation Results:

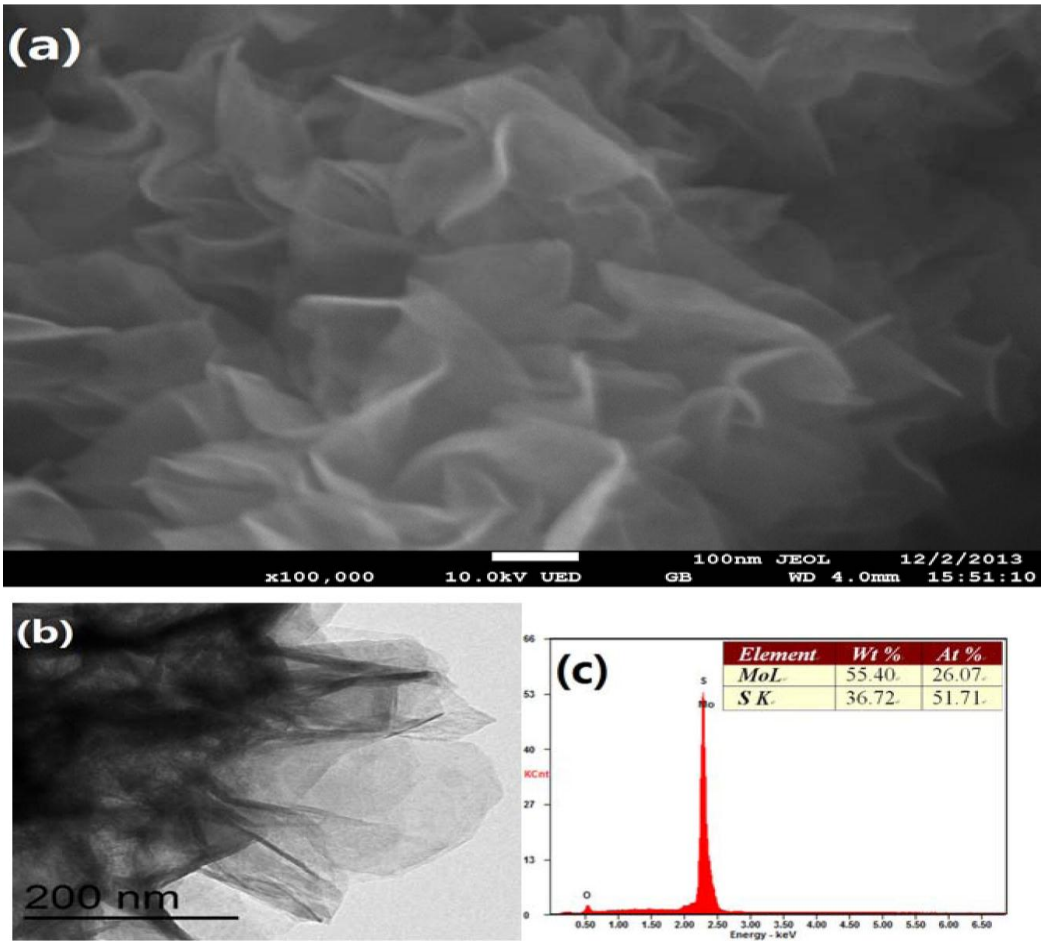

Fig. 3-7. (a) FESEM, (b) TEM images of sample C show curved sheet-like structure and uneven surface morphology on a large scale, and (c) EDX spectrum of sample C gives a mole ratio of S:Mo of 1.98, which is about the same value of the ratio of S:Mo for the precursors.[42]

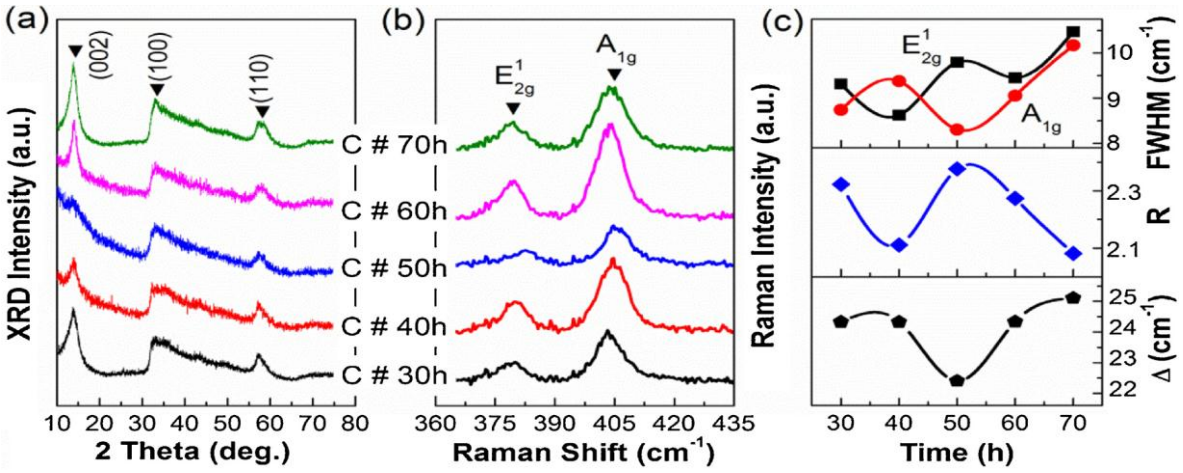

Fig. 3-8. (a) XRD patterns and (b) Raman spectra of sample C#30 h, C#40 h, C#50 h, C#60 h and C#70 h, which have the same ratio of precursors as that of sample C but undergo different hydrothermal time. (c) Full width at half maximums (FWHMs), relative intensities ($R = A_{1g}/E^1_{2g}$) and frequency differences ($D = A_{1g} - E^1_{2g}$) of their two characteristic Raman peaks A_{1g} and E^1_{2g}. [42]

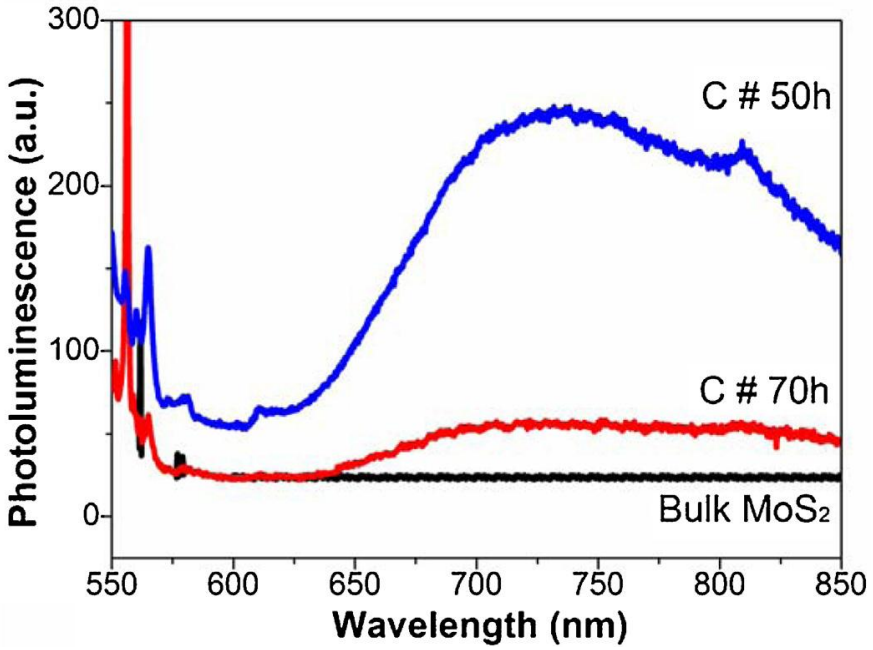

Fig. 3-9. Photoluminescence spectra of sample C#50 h, C#70 h and bulk MoS_2. An emerging broad photoluminescence in sample C#50 h indicates the bilayer or few layers of MoS_2 in the synthesized nanosheets. [42]

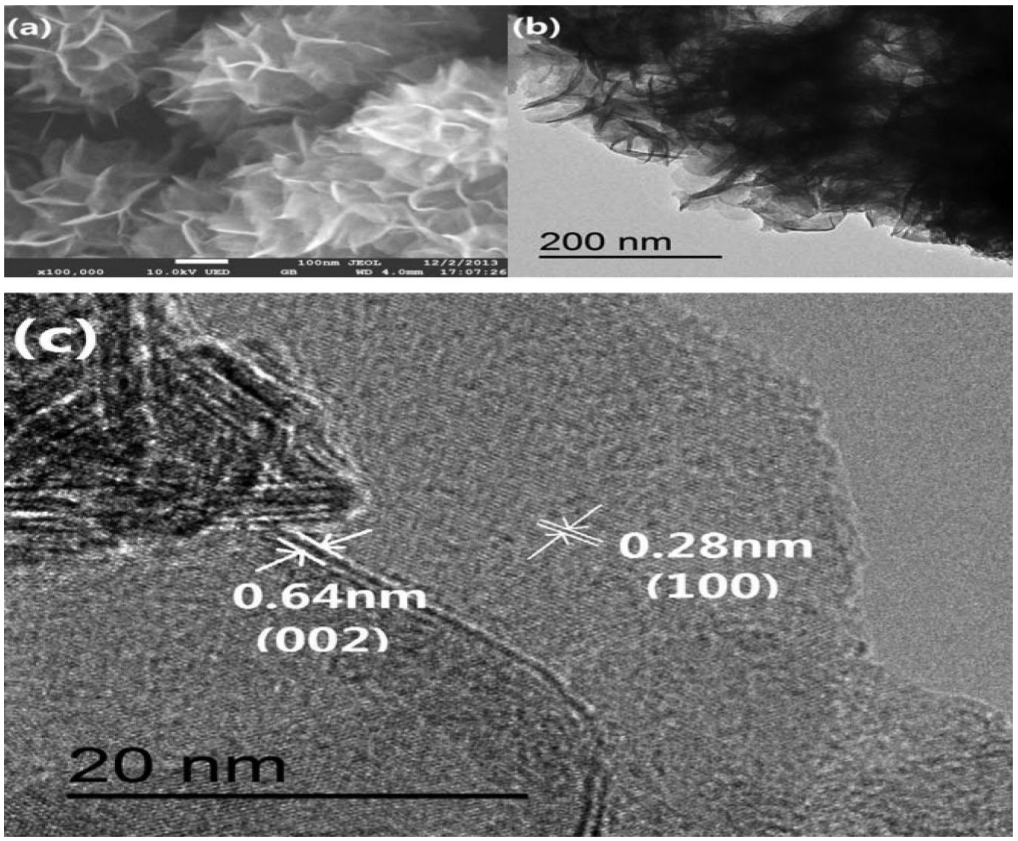

Fig. 3-10. (a) FESEM, (b) TEM and (c) HRTEM images of sample C#50 h prepared by using stoichiometric S and Mo precursors through hydrothermal processing for 50 h. [42]

Conclusion: MoS_2 nanosheets have been successfully prepared by a facial hydrothermal method with the sulfur and ammonium molybdate powders as starting materials. It was found that the thermal stability and crystalline quality of MoS_2 were significantly affected by the mole ratio of the precursor (molybdate and sulfur) and the hydrothermal time. When mole ratio of precursor is stoichiometric, then the as-prepared MoS_2 (sample C) showed the best crystalline quality and purity. These as-obtained bilayer MoS_2 nanosheets (sample C#50 h) are grown further in optimal hydrothermal time is found to display pronounced photoluminescence and also, possess high adsorption capacity because of the large surface area.

Title: Role of the Seeding Promoter in MoS_2 Growth by Chemical Vapor Deposition

Experimental Conditions: Xi Ling et al.[46] reported a CVD method for MoS_2 growth. 0.018g of MoO_3 (molybdenum oxide) powder is placed in a ceramic crucible in the center of furnace. Moreover, 0.016g of sulfur powder is placed in another crucible that is 15 cm away from the center of the quartz tube. Substrate is placed face-down on that crucible of MoO_3 powder. About 5 sccm Ar is used as a carrier gas. Growth temperature is controlled at 650 °C. The large-area, continuous MoS_2 monolayer can be generally achieved by using PTAS as the

seeding promoter.

Characterisation Results:

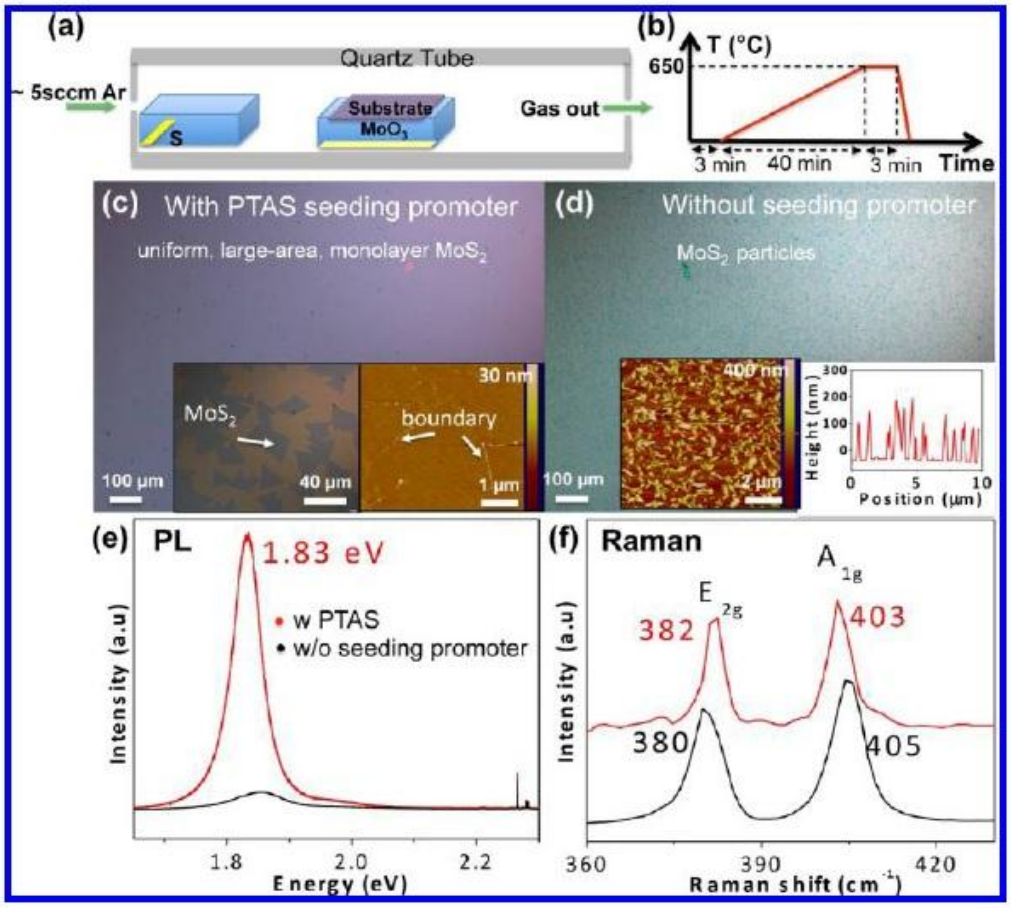

Figure 3-11. (a) A schematic illustration of the MoS_2 CVD system. (b) The temperature programming process used for a typical growth. (c–d) Typical growth results obtained with (c) and without (d) using PTAS as a seeding promoter. The insets in (c) are the optical image of the triangular MoS_2 flakes at the edge of the MoS_2 monolayer film, and the AFM image on the continuous MoS_2 monolayer film. The insets in (d) are the AFM image of the MoS_2 particles deposited on the surface and the corresponding height cross-section analysis. (e–f) Typical PL (e) and Raman (f) spectra of MoS_2 samples that were prepared with (red) and without (black) PTAS seeding promoter. The PL intensities are normalized by the intensities of the A1g Raman mode. The excitation wavelength is 532.5 nm. [46]

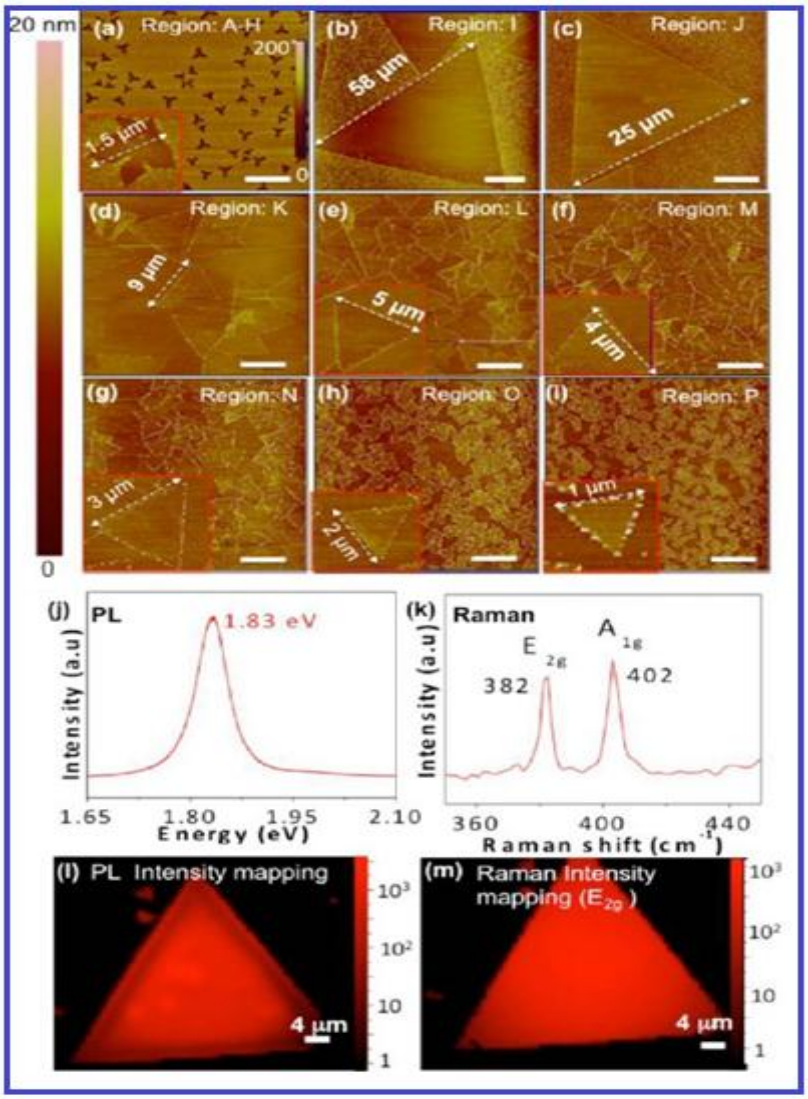

Figure 3-12 (a–i) AFM height images (except (a) which is the phase image) of MoS_2 domains on different regions of the growth substrate. The insets show the corresponding zoom in images. The domain sizes are marked on each of the images. Scale bar: 5 μm (except 10 μm in b). (j–k) Typical PL (j) and Raman (k) spectra of the triangular MoS_2 domains. (l–m) The mapping images of the intensity of PL (l) and E_{2g} Raman mode (m) of a triangular MoS_2 flake in the region J. The excitation wavelength is 532.5 nm. [46]

Conclusion: The excitation wavelength for Raman and PL measurement is typically 532.5 nm. Some of the spectra are taken by using a 632.8 nm wavelength.

By comparing the growth result with as well as without using PTAS seeding agent, it is obvious that a continuous, large-area, and superior quality MoS_2 monolayer can be synthesized under relatively low temperature (650 °C) conditions by using PTAS as a seeding enhancer, while only MoS_2 particles can be obtained by using the same growth conditions however without any seeding agent. Moreover, with the aid of a seeding promoter and thereby, examining the growth results on a substrate as a function of the distance between the growth regions and promoter substrate, it is shown that optimum seed concentration is necessary for the growth of the desired MoS_2 monolayer.

Lin Ma et al.[41] worked on the One-pot synthesis method of MoS_2 nanosheets .

Keng-Ku Liu et al.[12] reported that the high temperature annealing of a thermally decomposed ammonium thiomolybdate layer in the presence of sulfur can produce large-area MoS_2 thin layers with superior electrical performance on insulating substrates.

Lijuan Ye et al.[42] reported the Hydrothermal synthesis of MoS_2 nanosheets.

Yongjie Zhan et al.[21] devised the Large-Area Vapor-Phase Growth method of MoS_2 nanosheets

Yufei Yu et al.[44] reported high temperature synthesis method with solid precursors which led to successfully grown monolayer or few$layerMoS_2$ films on various substrates including silicon oxide, sapphire, and graphite and analysed them with the standard characterization techniques.

Kiran Kumar Amara et al. [45] reported on the preparation of mono- and bi-layer molybdenum disulfide (MoS_2) from a bulk crystal by facile wet chemical etching. Their findings indicate that the self-limiting chemical etching is a promising top-down route to preparing atomically thin crystals from bulk layer compounds.

Ling et al.[2] studied the dependence of the growth results on the seed concentration and in addition to the already identified seeding promoters,various other aromatic molecules were further investigated. In contrast, no enhancement in monolayer MoS_2 growth was observed when inorganic nanoparticles were used.

In their review, Yufei Zhao et al.[43] briefly summarizes the properties , structure and synthesis of MoS_2 as per their applications for H_2 generation and lithium ion batteries.

Sohail Ahmad et al.[47] studied the structural and electronic properties of MoS2 using plane wave pseudopotential method under GGA scheme based DFT calculations. They observed that not just the band gap of monolayer MoS_2 can be tuned by uniform strain, but also the direct to indirect and the semiconductor to metal transitions can be controlled.

Wu Zhou et al. [49] provide a systematic study of intrinsic structural defects in chemical vaporphase grown monolayer MoS2, including dislocations ,point defects, grain boundaries,

and edges, via the direct atomic resolution imaging, and explored their energy landscape and also their electronic properties

Nanjundan Ashok Kumar et al.[50] highlight the pivotal role of monolayered MoS_2 in sensing, electrochemical energy storage, hydrogen generation through photochemical water splitting and also, electronic device applications such as field-effect transistors. Perspectives on these challenges and the associated opportunities for the exploration of such 2D layered hybrid materials are put forward.

Wenjuan Zhu et al. [51] report the electronic transport and device properties of monolayer molybdenum disulphide grown by chemical vapour deposition method. They reported that these devices have enough potential to suppress short channel effects and have high critical breakdown electric field. However, their study highlights that the electronic properties of these devices are at present severely limited and continual engineering efforts are needed for its potential applications.

Arend M. Van der Zande et al. [52] reported to have used chemical vapor deposition synthesis with solid precursors for the growth of highly crystalline islands of monolayer molybdenum disulfide and further studied its optical and electrical properties.

Lei Yang et al. [16] introduce metal nanoparticles (Cr, Ag) to the surface of MoS_2 nanosheets by simple synthetic means creating a hybrid metal-MoS_2 nanosheet system with well-defined metal/ semiconductor interfaces. Further they demonstrated that this hybrid nanosheet structure is capable of decoupling the light absorption, chiefly in MoS_2, and also, carrier separation across the metal-MoS_2 heterostructure which leads to drastic quenching of recombination between photogenerated carriers in MoS_2.

In their paper, Kangho Lee et al. [55] reported the electrical characteristics of MoS_2 films and flakes, which have been produced through liquid phase exfoliation processing.

Ehren M. Mannebach et al.[56] report on the ultrafast electronic and structural dynamic response of single layer MoS_2 to intense above-bandgap photoexcitation.

Mono- or few-layered transition metal dichalcogenides — obtained either through exfoliation of bulk materials or bottom-up syntheses — are direct-gap semiconductors whose bandgap energy, as well as carrier type (p- or n-type), varies amongst compounds which depends on their composition, structure and dimensionality. Manish Chhowalla et al. [37] describe how their tunable electronic structure make them attractive for a variety of applications. These have been investigated as chemically active electrocatalysts for hydrogen evolution and hydrosulfurization, as well as electrically active materials in opto-electronics. Their properties and morphologies are also useful for energy storage applications such as electrodes for Li-ion batteries and supercapacitors.

R. Ansari et al.[53] explore the mechanical properties of a monolayer molybdenum disulfide (MoS_2). The results demonstrate that the elastic properties of MoS_2 nanosheets are less than those of grapheme. On the other hand, their Poisson's ratio is reported to be higher than that of graphene. It is also observed that due to the special structure of MoS_2, thickness of the nanosheet alters when the axial strain is applied.

Jia Zhang et al.[54] synthesized edge-oriented MoS_2 nanosheet-like films that exhibit weak magnetism and magnetoresistance effects. Their calculations in order to provide insight into the origin of this magnetism imply that nanostructured films with a high density of edge spins can give rise to magnetism even though the bulk material is nonmagnetic.

Sina Najmaei et al.[16] use self-assembled monolayers with a variety of end termination chemistries to functionalize substrates and systematically study their influence on the physical properties of MoS_2.

4 Choice of Method Amongst Available Synthesis Methods of Monolayer Molybdenum Disulphide : CVD

Amidst the numerous methods reported to grow or fabricate monolayer MoS_2, some of them have been very successful attempts. With reference to our aim to implement a controllable growth method, focus was on the bottom-up approaches, leaving aside the top-down approaches like lithium intercalation assisted exfoliation and mechanical exfoliation which exercise minimal control on the thickness of layers. Hence, a detailed study of the pros and cons of these bottom-up methods lead to the conclusion of chemical vapour deposition as the chosen chemical route for the synthesis procedure adopted by this project.

There are several deposition techniques which take place in the liquid phase, where ionic precursors and reactants in aqueous form are used to synthesize monolayer MoS_2. Such techniques include thermolysis, electrochemical and hydrothermal methods. Two of the more simple liquid phase methods are briefly enumerated below.

4.1 Electrochemical Synthesis

A two-step electrochemical/chemical synthesis of 2H-MoS_2 was designed by *Q. Li et al.* [11] It was done by electrodeposition of MoO_2 nanowires onto highly oriented pyrolytic graphite surfaces, prior to exposing them to hydrogen sulphide at elevated temperatures in order to reduce MoO_2 into the desired MoS_2 form. The risk factor involved in this method is high as the use of H_2S at high temperatures has to be carried out with utmost caution, if it were to be adopted as an industrial process. H_2S in high quantities is highly poisonous and is a strong factor to consider in choosing an appropriately safe growth method.

4.2 Thermolysis of Ammonium Thiomolybdates

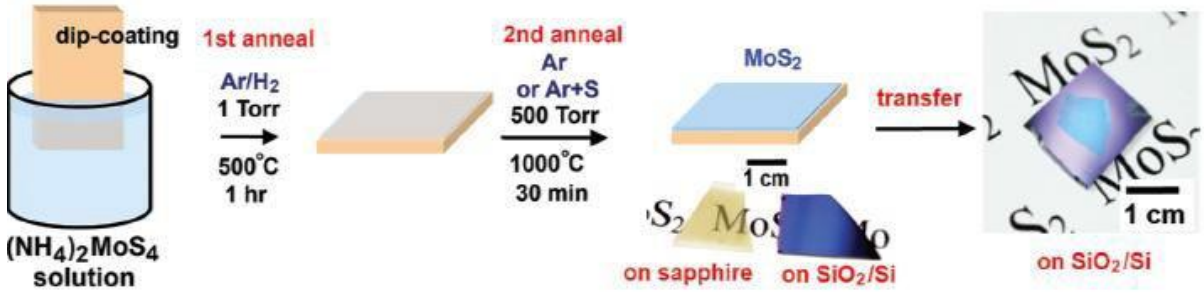

Figure 4.1 Two-step thermolysis of ammonium thiomolybdate.[12]

K. Liu et al.[12] developed this two step thermolysis method of ammonium thiomolybdate. Here, ammonium thiomolybdate coated on an insulating substrate like SiO_2/Si is annealed twice to facilitate reduction in order to form MoS_2 trilayers. Though this method appears reliable and simple, the requirement for high temperatures and formation of multilayer MoS_2 during synthesis poses as a drawback.

As the intention is to fabricate monolayer MoS_2 with relatively lower temperatures and simpler pressure requirements , these methods do not serve the purpose. Hence, other more suitable methods are sought after.

4.3 Physical Vapour Deposition

There are also techniques which require reactants and precursors in the vapour phase, namely physical or chemical vapour deposition. Physical vapour deposition encompasses pulsed layer deposition, thermal or electron beam evaporation, van der Waals , molecular beam epitaxy and sputtering. However, only thermal evaporation has been found to be widely used because of its low equipment requirements and relatively simple experimental set up. Following are some of the more feasible techniques considered during the course of selection of synthesis route.

In a method followed by *C. Gong et al.* [13], a source of MoS_2 powder is placed in a quartz tube which is residing in a furnace, with the insulating substrate placed downstream. The temperature of the furnace is around 650 ºC. The source is heated for approximately 15-20 min at a temperature of about 900 ºC with Ar gas flowing at base

pressure of 20 mTorr to maintain an inert atmosphere. Such high temperature requirements for heating are definitely a big concern for the purpose of designing a low cost process. The relatively low temperature of 600 ºC required for condensation on a substrate is also difficult to achieve in small furnace set ups where most of the furnace would be at one temperature or at an indeterminable range of high temperatures.

Thus, this method too does not fulfill all our requirements and further methods are to be investigated.

4.4 Chemical Vapour Deposition

After much research and analysis of the works being carried out on nanosheets of MoS_2 around the globe, chemical vapour deposition has been chosen as the means of fabricating monolayer MoS_2. The following section provides an insight to the theory behind CVD, at length.

4.4.1 Different Reaction Zones

During the deposition process, five reaction zones are formed there in the furnace as shown in Figure 4.2 below. These zones play distinctly important roles in the entire process.

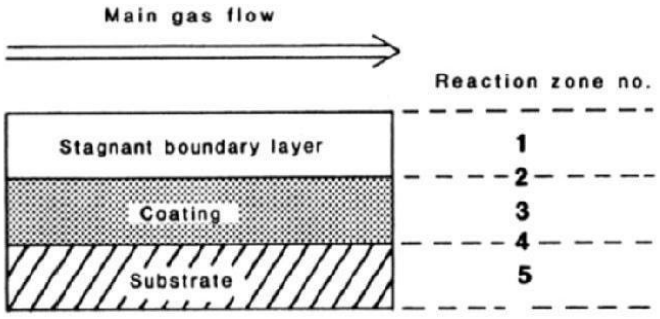

Figure 4.2 Reaction zones during CVD.[26]

Homogeneous nucleation as well as the main gas stream occurs in Zone 1. Whereas the heterogeneous reactions occur in Zone 2, which is the interface between stagnant boundary layer and coating. The reactions in these zones seem to have an effect on the deposition rate as well as the properties of the coating.[26]

4.4.2 Physiochemical Steps

The process involving CVD growth generally, in entirety, takes place in 6 steps. Firstly, the reagents are transported through the stream of the main gas flow. Secondly, the reagents are found to undergo a variety of different gaseous phase reactions in the different reaction zones in order to produce a number of reaction intermediates as well as by-products. Thirdly, the reactants are transported to the surface of substrate. Fourthly, adsorption to the substrate surface takes place. Fifthly, it is observed that nucleation, surface diffusion and many more reactions occur on the surface.

Finally, the volatile products that are left behind, are desorbed and transported away from the reaction zone along the outgoing main gas flow.[27] These steps have been depicted in Figure 4-3 below.

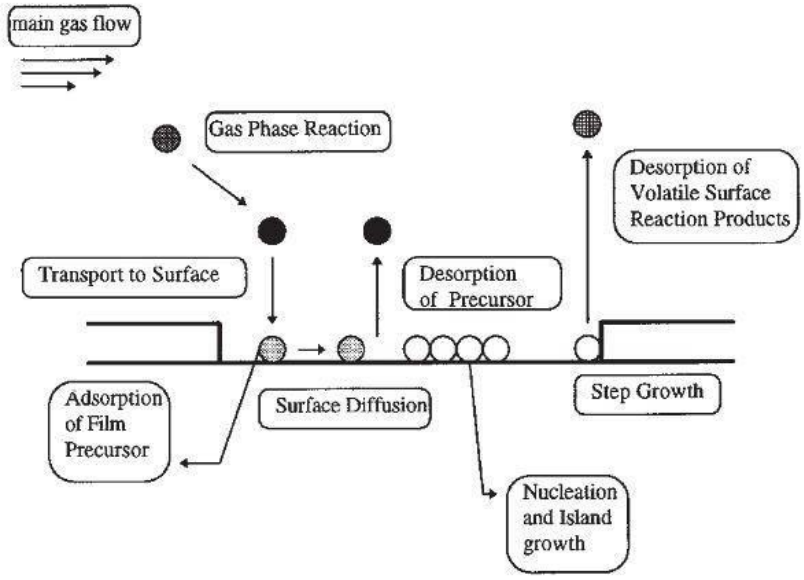

Figure 4.3 Physiochemical steps of CVD.[27]

4.4.3 Adhesion

Successful growths by CVD necessitates the well adhesion of the grown coating upon the substrate surface. A multitude of factors play a pivotal role in this regard, as reported by A. C. Jones [27] .

Stress is one such factor. Deposition stress as well as mismatch of the thermal expansion coefficients during the process of heating or cooling are some of the factors that can

adversely affect the adhesive properties of the grown substance. In order to counteract this situation, the substrate should be left to cool naturally, on its own and slowly within the closed furnace after each and every experiment.

Another factor found is homogeneous nucleation. This results in a powdery deposit across the substrate, and thereby, thin film growth cannot be obtained. The free energy of heterogeneous nucleation is expressed in Equation 5.3.1 [31,32] below.

$$\Delta G_{Hetero} = \Delta G_{Homo} f(\theta);$$
$$f(\theta)=(1/2)-(3/4)\cos\theta+(1/4)\cos^3\theta \quad ...5.3.1$$

The contact angle θ in the above equation represents the angle subtended between the growing substance and nucleation site. Since f(θ) varies, mathematically, from one to half to zero as the contact angle, θ varies from 180º to 90º to 0º, it becomes apparent that the free energy associated with heterogeneous nucleation also drops to zero as the contact angle decreases upto zero. This implies that wetting of the surface leads to increase in heterogeneous nucleation. This is in line with the observations made of seeding as being beneficial to the growth of MoS_2 as seen in Chapter 3.[30]

The formation of boundaries or cracks in the growth may also be facilitated by the formation of pores in the substrate or the coating. However, this can be minimised with simple substrate cleaning procedures.

4.4.4 Role of Precursor and Growth Volatility

Since the precursors that can be used in this experiment will be in solid form, their volatility is, obviously, of natural importance. A good estimate of the temperature required to vaporise can be obtained by relevant studies made by other research groups around the globe, and also from the thermogravimetric analysis (TGA) data. TGA provides an insight into the modulation of certain properties of a material with respect to temperature. For instance, in Figure 4.4 below, the graphs highlight how much mass of solid MoS_2 is lost or vaporized, as temperature is increased.

One noteworthy interesting point is that the TGA data for the end product, MoS_2, indicates more volatility in its nanoscale structures as compared to its bulk counterpart.

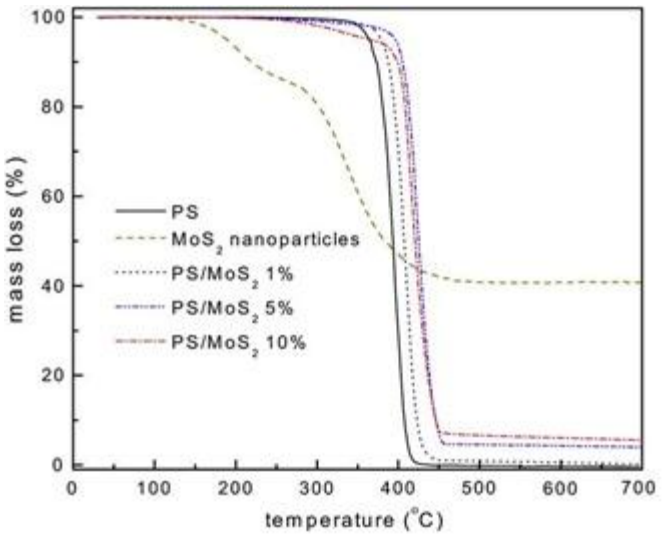

Figure 4.4. TGA data of MoS_2 nanoparticles and other mixed compounds [28].

The comparison in Figure 4.4 shows the expected TGA curve for MoS_2 nanoparticles alongwith its bulk counterpart with the 0% curve. While MoS_2 nanoparticles are found to begin evaporating at much lower temperature, about 200ºC, its bulk counterparts do so in a relatively higher temperature, about 400 ºC. In a study headed by *Xin Lu et. al.* [33], MoS_2 underwent layer-by-layer thinning when it was thermally annealed. The group annealed samples at a temperature of 650 ºC for one hour per cycle. This led them to the observation of the loss of one layer per cycle. These are strong evidences that hint that MoS_2 monolayers may still be relatively volatile, even after the processes of surface adsorption and adhesion have occurred.

4.4.5 Overview of Contemporary Work on CVD

CVD methods in association with synthesis of MoS_2 nanosheets mainly comprise of sulphurization of Mo reactants in various forms. Different forms of Mo compounds can be used as precursors for CVD. One may use its oxide as MoO_3, metal form Mo, or even $MoCl_5$. These may appear in different physical forms, such as a thin metal film deposited on a substrate, or as nanorods. Here, an insight is provided at specific aspects of the CVD growth process that are common amongst many research groups attempting to fabricate monolayer MoS_2.

(1) Temperature and Pressure

It has been observed that the research groups that simply stuck to use high purity MoO_3 and S powders had to use slightly elevated furnace temperatures of approximately 750 ºC to 950 ºC [4,15-17]. However, when seeding was involved or when the precursor used is a less conventional form like Mo thin film or ammonium thiomolybdate, then the growth process usually requires a relatively lower temperature between 400 ºC to 750 ºC [15,19,21] approximately.

CVD methods mainly comprise of sulphurization of Mo reactants in various forms. Different forms of Mo compounds can be used as precursors for CVD. One may use its oxide as MoO_3, metal form Mo, or even $MoCl_5$. These may appear in different physical forms, such as a thin metal film deposited on a substrate, or as nanorods. Here, an insight is provided at specific aspects of the CVD growth process that are common amongst many research groups attempting to fabricate monolayer MoS_2.

(2) Seeding and Controlled Nucleation

Around the globe, several research groups have employed seeding methods to enhance the nucleation and growth of MoS_2.

In a method employed by *Y. Lee et al.* [14], seeding agents such as, reduced graphene oxide (rGO), perylene-3,4,9,10- tetracarboxylic dianhydride (PTCDA) and perylene-3,4,9,10-tetracarboxylic acid tetrapotassium salt (PTAS) were used to treat the substrate prior to the growth process. For rGO, a GO solution is mixed with hydrazine and heated to cause the reduction, before a drop of rGO-hydrazine is spin coated onto the substrate. PTAS and PTCDA were also used similarly in separate experiments in order to spin coat the substrate prior to the CVD growth and successfully promote MoS_2 flake growth[15].

One group headed by S. Najmaei[16] chose to manipulate the substrate surface, in order to provide low energy locations for easier nucleation sites for MoS_2. They used lithography to pattern the rectangular SiO_2 pillars to achieve a high density of nucleation sites and

subsequently, the formation of large-area MoS_2 films.

Another group made use of the intermediate reduction product of MoO_3 to MoO_2 as the nucleation structures. *X.Wang et al.*[17] allowed the MoO_2 rhomboidal microplates to form, before further annealing was carried out on their surfaces and reduced to MoS_2 with multiple layers which depended on the annealing time.

Moreover, there were a few groups which focussed on using clean substrates and not using any seeding agents whatsoever[4].

(3) Precursor, Reactant and Gas Flow

In terms of reactants, a majority of groups were found to adhere to the use of high purity MoO_3 and sulphur powder respectively[4,15-17]. However, there were certain groups which used different starting precursors.

X.Shi et al. [19], used ammonium thiomolybdate in vapour form as a precursor, and which is carried to a graphene surface with the aid of a carrier gas prior to annealing for thermal decomposition of the precursor into epitaxial MoS_2 flakes on graphene.

$MoCl_5$ powder and sulphur powder were used as precursor and reactant respectively by *Y. Yu et al.*[20]. They grew high quality thin film of MoS_2 at a high temperature of 850ºC and a low pressure of 2 Torr. Also, they varied the number of layers grown by altering the amount of precursor used or the total pressure exerted.

Y.Zhan et al. [21] is reported to have deposited Mo thin films onto SiO_2 substrates and sulphurized them directly with sulphur vapour.

5 Methods of Characterization

Characterization techniques are referred to those methods through which one can identify an as-prepared sample with respect to its morphology, surface topology, internal structure, composition, etc. The characterization techniques used to study a sample, depends on its properties, features, tolerance to the imposed environment so that during the process, no damage is done to the sample either internally or externally.

In order to analyse the as-grown MoS_2 samples, a few tools capable of characterising them at a microscopic scale were necessary as the crystal compound growths were expected to be up to several micrometres in size. On account of the focus upon streamlining the growth process and thereby, obtaining single layer growths, the following powerful techniques of characterizing the samples were necessitated. The set up and working of these techniques are briefly summarized below: Optical Microscopy and Raman Spectroscopy. Although the Atomic Force Microscopy (AFM) was initially used to characterise sample thickness, the study by C. Lee et al. deemed that Raman spectroscopy was accurate enough for determining layer thickness[3].

5.1 Atomic Force Microscopy (AFM)

It is a very high-resolution kind of scanning probe microscope (SPM), with demonstrated resolution of the order of fractions of a nanometer. It provides images to the users with atomic or near-atomic resolution surface topography; also it is capable of quantifying surface roughness of samples upto the angstrom scale. In a field of semiconductor physics, studies have been made on,for example, (a) an identification of atoms at a surface, (b) the evaluation of interaction between a specific atom and its neighboring atoms and (c) a change in physical properties arisen from a change in an atomic arrangement thorough the atomic manipulation.
AFM typically consists of following features:

1. Cantilever (1) : Small spring-like cantilever(1)which is supported on the support (2) by means of a piezoelectric element (3) which is used to oscillate the cantilever (1) at its eigen frequency ;
2. Sharp tip (4) which is fixed to the open end of the cantilever (1) .
3. Detector (5) is configured to detect the deflection and motion of the cantilever (1) .
4. Sample (6) will be measured by AFM are mounted on the Sample stage (8).

5. xyz-drive (7) which permits a sample (6) and the Sample stage (8) to be displaced in the x, y, and z directions with respect to a fixed tip apex(4).

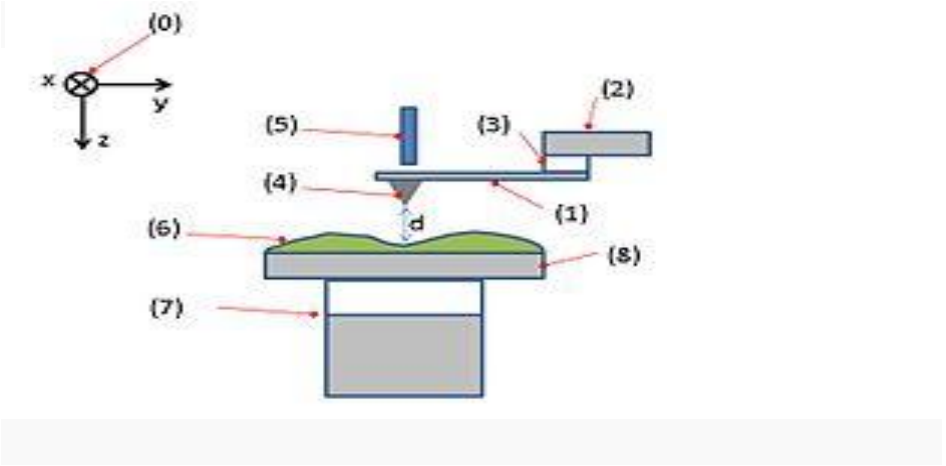

Figure 5.1. Typical configuration of AFM

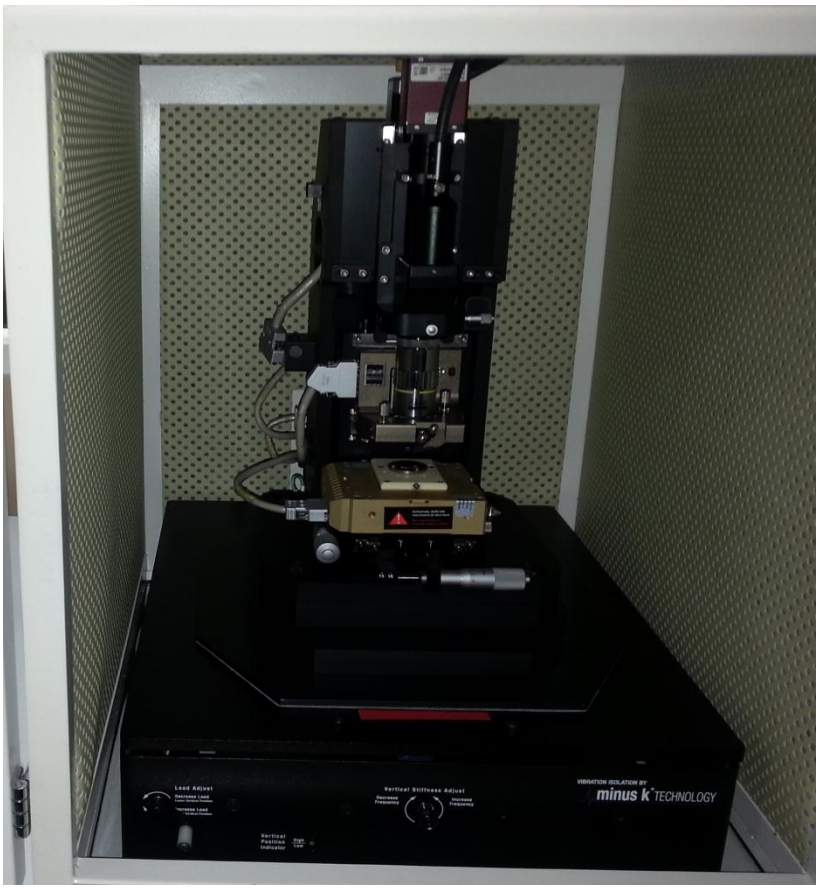

Figure 5.2. Picture of AFM setup @DTU

The AFM consists of a cantilever having a sharp tip (probe) at its end that is used to scan the surface of specimen. Typically the cantilever is made of silicon or silicon nitride with the radius of curvature of the tip of the order of nanometers. It is observed that when the tip is brought into the vicinity of a sample surface, forces between the tip and the sample act such

that they lead to a deflection of the cantilever. Typically, the deflection is measured with the help of a laser spot reflected from the top surface of the cantilever into an array of photodiodes. AFM operates in three different modes, namely, tapping mode, contact mode, and non-contact mode.

Contact Mode

In contact mode, the tip is "dragged" across the surface of the sample and the contours of the surface are measured either by using the deflection of the cantilever directly or, more commonly,by using the feedback signal that is required to keep the cantilever at a constant position. As the measurement of a static signal is prone to the noise and drift, low stiffness cantilevers (i.e. cantilevers having a low spring constant, k) are used to boost up the deflection signal. When at close proximity to the surface of the sample, the attractive forces can be relative strong, resulting the tip to "snap-in" to the surface. Hence, contact mode of AFM is almost always done at a depth whereby the overall force is repulsive, that is, in firm "contact" with the solid surface that is below any adsorbed layers.

Tapping Mode

In tapping mode, the cantilever is driven to oscillate up and down around its resonance frequency with the aid of a small piezoelectric element mounted in the AFM tip holder similar to that in non-contact mode. The interaction of the forces like, dipole-dipole interactions, Van der Waals forces, electrostatic forces, etc. acting on the cantilever when the tip comes close to the surface, cause the amplitude of this oscillation to decrease as the tip gets more and more close to the sample. The electronic servo uses piezoelectric actuator in order to control the height of the cantilever above the sample. The servo adjusts the height such as to maintain a set cantilever oscillation amplitude as the cantilever scans over the sample. A tapping AFM image is thus produced by imaging the force of the intermittent contacts of the tip with the surface of the sample.

This method of "tapping" lessens the damage done to the surface and the tip compared to the amount done in contact mode.

Non-Contact Mode

In non-contact atomic force microscopy mode, the tip of the cantilever does not come in contact with the surface of sample. Instead, cantilever is oscillated at either its resonant frequency (frequency modulation) or just above (amplitude modulation) where the oscillation

amplitude is typically a few nanometers (<10 nm) down to a few picometers. The van der Waals forces, being strongest in the range of 1 nm to 10 nm above surface, or some other long-range force which extends above the surface tends to decrease the resonance frequency of the cantilever. The decrease in the resonant frequency alongwith with the feedback loop system maintains a constant oscillation amplitude or frequency by continually adjusting the average tip-to-the sample distance. When the tip-to-sample distance is measured at each (x,y) data point,it allows the scanning software to construct a topographic image of the sample surface.
Non-contact mode AFM does not suffer from tip or sample degradation effects which are sometimes observed after taking numerous scans with contact AFM. This is why non-contact AFM are preferred to contact AFM for measuring soft samples.
For samples grown for this project, the tapping mode was used to image samples, which is the least destructive mode of three operating modes.

5.2 Scanning Electron Microscopy (SEM)

It is a kind of electron microscope that produces images of a sample by scanning the sample with a focussed beam of electrons. The electrons interact with the atoms in the sample, thereby producing a variety of signals that can be detected and that contain information about the sample's surface topography and composition. The electron beam is normally scanned in a raster scan pattern, while the beam's position is typically combined with the detected signal to produce an image. SEM can achieve resolution finer than 1 nanometer.

The most common SEM mode is the detection of secondary electrons emitted by atoms which are excited by the beam of electron. The number of the secondary electrons depends on the angle at which beam meets specimen surface, i.e. on specimen topography. By scanning the sample and collecting the secondary electrons with the help of special detector, the image displaying the topography of the particular surface is formed, revealing minute details less than 1 nm in size.

SEM is typically consisted of the following features:

- A source (electron gun) of the electron beam which is accelerated down the column.
- A series of lenses(condenser and objective) which act to control the diameter of the beam and also to focus the beam on the specimen

- A series of apertures (micro scale holes in metal films) through which the beam passes and which affects properties of that beam
- Controls for specimen position (x,y,z-height) as well as orientation (tilt, rotation);
- An area of beam/interaction which generates several types of signals that can be detected and processed so as to produce an image or spectra; and
- All the above are maintained at high vacuum levels.

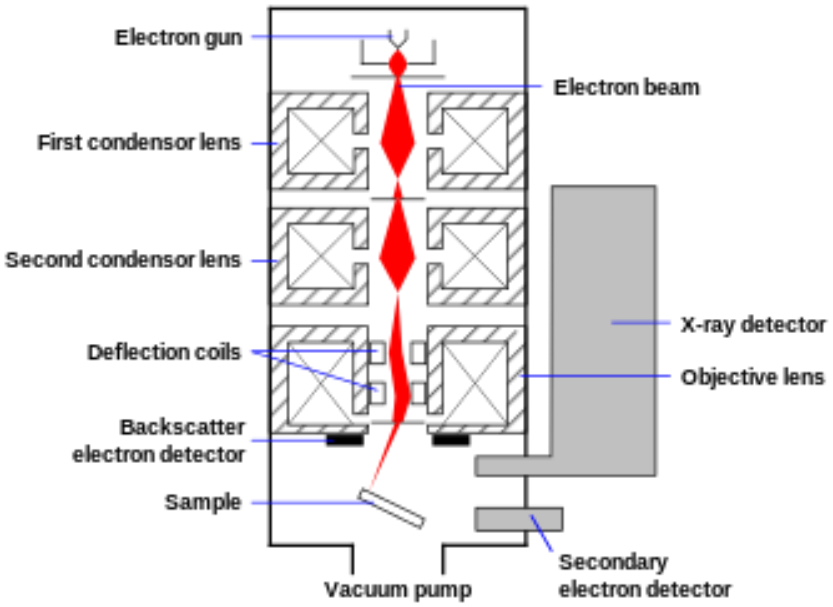

Figure 5.3. Schematic setup of SEM apparatus

Figure 5.4. Picture of SEM setup @DTU

Typically, in a SEM, an electron beam is thermionically emitted from an electron gun that is fitted with a tungsten filament cathode. The electron beam, which has an energy which typically ranges from 0.2 keV upto 40 keV, is generally focussed by one or may be, two condenser lenses to a spot that is about 0.4 nm to 5 nm in diameter. The beam then passes through pairs of scanning coils or pairs of deflector plates present in the electron column, typically in the final lens, which then deflects the beam in the *x* and *y* axes such that it scans in a raster fashion over a rectangular area of the sample surface. The beam is rastered from left to right and top to bottom. There is a direct one-to-one correspondence between the rastering pattern of the specimen and the rastering pattern that is used to produce the image on the monitor. The resolution chosen to image affects the number of pixels per row as well as the total number of rows that constitute the scanned area. When the primary beam of electrons interacts with the sample, the electrons lose their energy by repeated random scattering and absorption within the interaction volume, that extends from lesser than 100 nm to 5 µm approximately into the surface. The types of signals produced by a SEM include back-scattered electrons (BSE), secondary electrons (SE), characteristic X-rays ,Auger electrons, light (cathodoluminescence) (CL).

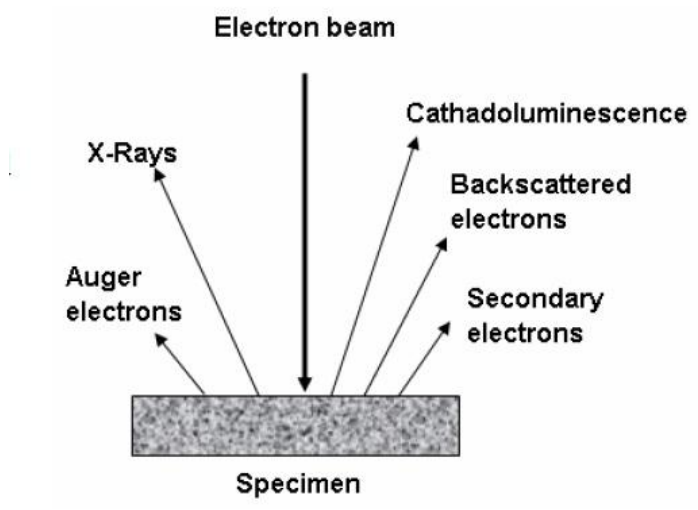

Figure 5.5. Types of electrons released during SEM imaging

1) **Secondary Electrons**: If an incident electron collides with an electron in a sample atom, it will knock that electron out of its orbital shell and the atom becomes ionised. Because the incident electron loses only a little energy during each collision, hence, multiple collisions are possible, continuing until the incident electron has no more energy to dislodge secondary electrons. Each freed secondary electron has a small kinetic energy (<50 eV), and this energy is independent of the energy of the incident electron. If generated close enough to the sample

surface (<10 nm), these secondary electrons can escape from the sample and can be collected by the detector. As a result, secondary electron imaging is closely related to sample topography.

2) **Backscattered Electrons**: If an incident electron collides with the nucleus of a surface atom, then the electron will bounce back or scatter 'backward' out of the sample as a backscattered electron (BSE). These electrons have high energies, typically in the range of 50 eV and that of the original incident electron. The production of these backscattered electrons varies directly with atomic number, and thus backscattered electron images can be used in order to discern differences in sample atomic number.

3) **Auger Electrons**: As a result of generation of secondary electron, a vacancy is left in an ionised atom's electron shell. In order to fill this vacancy, an electron from a higher energy outer shell (from the same atom) can drop down to fill the vacancy. This creates a surplus energy in the atom that can be corrected by emitting an outer electron, which is an Auger electron. Auger electrons have a characteristic energy unique to the element from which they are emitted and hence, can be used to give compositional information about the target sample. However, Auger electrons have a relatively low kinetic energy and are only emitted from shallow sample depths (<3 nm).

4) **Characteristic X-rays**: X-rays are also produced due to interactions of the incident electron beam with the surface of the sample. Similar to the process of Auger electron generation, the excess energy produced as a result of reshuffling electrons to fill shell vacancies can also be emitted in the form of an X-ray rather than an Auger electron. X-rays have a characteristic energy unique to the element from which they are emitted and so provide compositional information about the sample.
In order to characterize the as-grown samples in this project, were characterized using back-scattered electrons.

5.3 Photo Luminescence (PL)

This technique provides a non-destructive ,contactless means for obtaining identification of certain chemical impurities in semiconductors, and also, comparison of spectral sharpness of PL features which are associated with the recombination of free and bound excitons provides a

qualitative measure of crystal quality. Photoluminescence is a process in which an atom absorbs a photon of light resulting in the transition to higher electronic energy state and emits photon while returns back to the lower energy state.
When light of sufficient energy is incident on a material, the photons are absorbed and thus,

electronic excitations are created. These excitations relax eventually and the electrons return to the ground state. If the radiative relaxation occurs, then the emitted light is called PL. The PL signal itself is characterized by three essential features: energy, intensity, and polarization. This light can be collected and analyzed to yield a wealth of information about the photoexcited material. A given impurity produces a set of characteristic spectral features, whereby, this fingerprint identifies the impurity type, and most often several different impurities can be observed in a single PL spectrum. In another use, the half widths of PL peaks are an indication of sample quality and crystallinity. Features of the emission spectrum can be used to identify interface, surface, and impurity levels and also, to gauge interface roughness and alloy disorder. The information on the quality of interfaces and surfaces is provided by the intensity of the PL signal. The intensity and spectral content of the emitted photoluminescence is a direct measure of various important material properties, which includes:

Bandgap Determination: The spectral distribution of PL from a semiconductor can be analyzed to nondestructively determine the electronic bandgap. This is a means to quantify the elementary composition of compound semiconductor and is a vitally important material parameter influencing solar cell device efficiency.

Impurity Levels and Defect Detection: Low sample temperature PL spectrum often reveals spectral peaks associated with impurities contained within the host material. High sensitivity of the technique provides the potential to identify extremely low concentrations of intentional and unintentional impurities that can strongly affect material quality and device performance.

Recombination Mechanisms: The quantity of PL emitted from a material is directly related to the relative amount of nonradiative and radiative recombination rates. The nonradiative rates are generally associated with the impurities and hence, this technique can monitor qualitatively the changes in material quality as a function of growth and processing conditions.

PL is simple, versatile, and nondestructive. Instrumentation required for ordinary PL work is modest: an optical source and an optical power meter or spectrophotometer. Because the

measurement does not rely on electrical excitation or detection, the sample preparation is thereby, minimal. This striking feature makes PL relatively attractive for material systems having poor conductivity or undeveloped contact/junction technology.

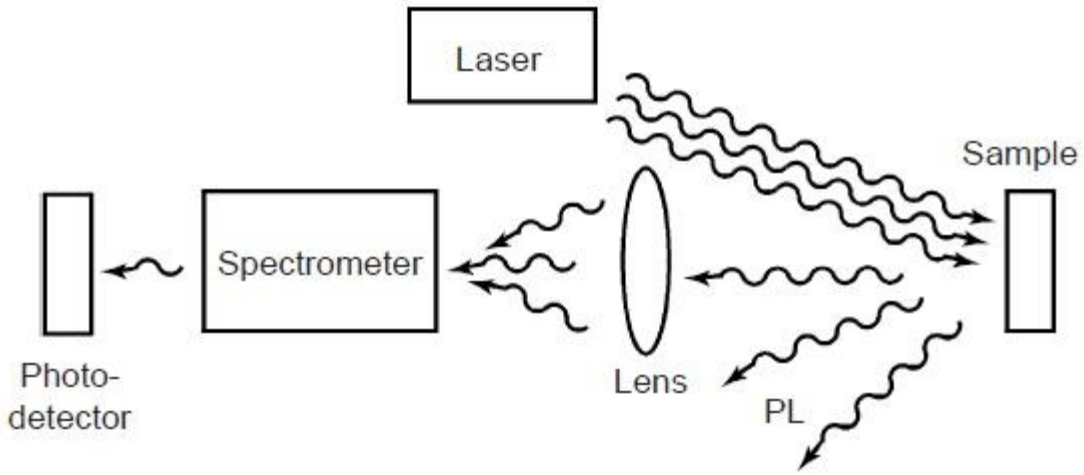

Figure 5.6. Schematic of PL setup

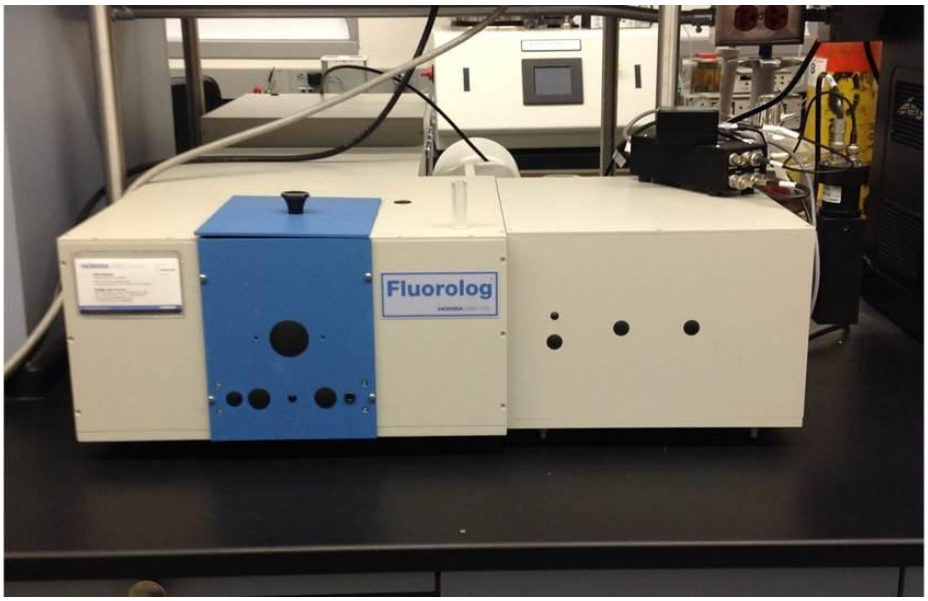

Figure 5.7. Picture of PL setup @DTU

In this experimental technique, laser with tunable wavelength and powers was used. Laser was guided to the sample by a set of mirrors and lenses. In order to keep the sample at relatively lower temperature the samples were placed in a closed cycle liquid helium cryostat, which can operate between 10 K and 300 K and is especially designed for PL measurements. PL signal was focused to the monochromator by means of lenses. In order to avoid the unwanted signals and noise different filters were used. The PL signal then passes through a single-grating monochromator which selects a wavelength to transmit to detector. The system is computer

controlled. Two types of detectors could be used at the exit slit of monochromator depending upon the signal to be detected. Normally at longer wavelengths photomultiplier tube is used and germanium photodiodes are good for the near-infrared range (1.1-1.8 μm, 0.7-1.1 eV). For the best signal-to-noise ratio these detectors should be operated at low temperature. A popular way of cooling the detector is by using liquid nitrogen. The signal was finally transmitted to a computer. Lock-in amplifier was used to measure the amplitude and phase of signals buried by noise. Signal from the lock-in amplifier and detector is obtained by the data acquisition board.

Photoluminescence spectra is used to characterise monolayer MoS_2. Multilayer MoS_2 would result in a weak PL due to its indirect band gap, while a monolayer sample should exhibit strong intensity direct band transitions at around 660 nm[2,18,25].

5.4 Ultraviolet Spectroscopy

Ultraviolet–visible spectroscopy (**UV-Vis** or **UV/Vis**) refers to the absorption spectroscopy or the reflectance spectroscopy in ultraviolet-visible spectral regime. This means that it uses light in the visible and its adjacent (near-UV and also, near-infrared (NIR)) ranges. The absorption or reflectance in this visible range directly affects the perceived colour of the associated chemicals. In this region of electromagnetic spectrum, the molecules undergo electronic transitions.

Molecules consisting of π-electrons or non-bonding electrons (n-electrons) are able to absorb energy in the form of ultraviolet or visible light in order to excite these electrons to the higher anti-bonding molecular orbitals. It is to be noted that, the more easily excited the electrons (i.e. lower the energy gap between HOMO and LUMO), longer the wavelength of light that it can absorb.

The absorbance or optical density of the molecule which is absorbing in UV or in visible region strongly depends on the molecular structure and its concentration is given by the Beer-Lambert relation

$$A = \log (I_0 / I) = Ebc$$

Where, I_0 and I denote the intensities of the incident and the transmitted radiation respectively, E is the molar absorptivity, b is pathlength, c is the concentration expressed in g moles/litre.

The basic parts of a spectrophotometer are, namely,

- a light source,
- a holder for the sample,
- a diffraction grating in a monochromator or a prism to separate the various wavelengths of light, and
- a detector.

The radiation source is most often a Tungsten filament (300-2500 nm),), Xenon arc lamp, being continuous from 160-2,000 nm; a deuterium arc lamp, being continuous over the ultraviolet region (190-400 nmor most recently, light emitting diodes (LED) for visible wavelengths. The detector is commonly a photomultiplier tube, a photodiode array, a photodiode, or a charge-coupled device (CCD). Single photodiode detectors as well as photomultiplier tubes are used with scanning monochromators, which filter the incoming light so that only light of a single wavelength is allowed to reach the detector at one specific time. Scanning monochromator is used to move the diffraction grating to "step-through" each and every wavelength so that its intensity can be measured as a function of the associated wavelength. It is observed that fixed monochromators are used with photodiode arrays and CCDs. As both consist of multiple detectors grouped in to one or two dimensional arrays, they are capable of collecting light of different wavelengths on different pixels or groups of pixels simultaneously.

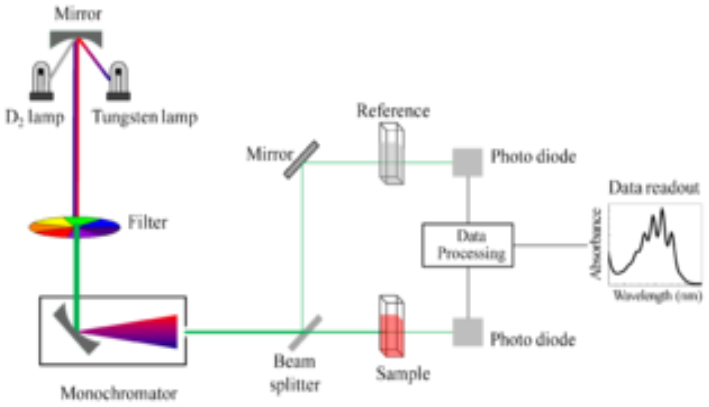

Figure 5.8. Schematic of UV- visible spectrophotometer.

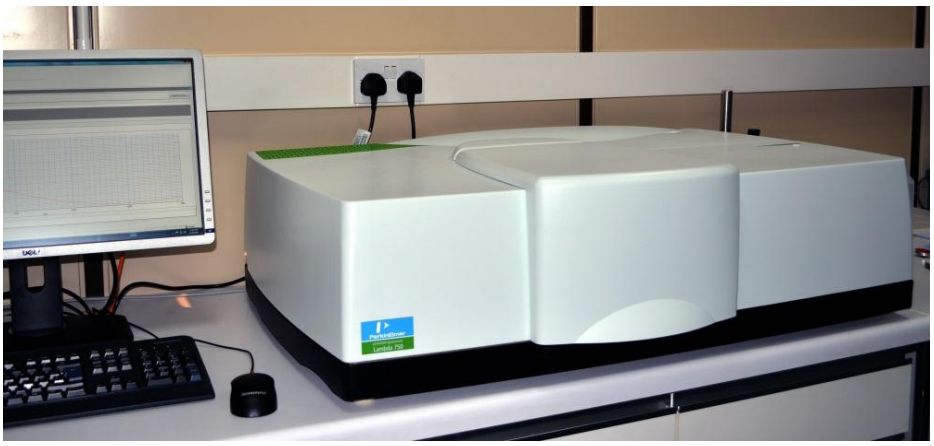

Figure 5.9. Picture of UV-Vis setup @DTU

A spectrophotometer can be either of single beam or double beam. In the single beam instrument, the entire light passes through the sample cell. I_0 has to be measured by removing the sample. This was earliest of all the designs and it still finds use in both teaching and industrial labs.

In the double-beam instrument, the light is splitted into two beams before it reaches the sample. Here, one beam is used as the reference; while the other beam passes through the sample. The reference beam intensity is considered as 100% Transmission (or 0% Absorbance), and the measurement is displayed as the ratio of the two beam intensities.

6 Experiment: CVD of Monolayer MoS_2

This chapter expounds on the entire experimental process at length, that has been undertaken in developing an inexpensive and reliable method of growing monolayer MoS_2.

6.1 Early Work

In the early stage of the work, without any prior experience in synthesising this particular compound, attempts were made by taking reference from the methods employed by the research groups as mentioned in chapter 4 above[4,15-17]. It was decided to attempt CVD with the popular precursor and reactant, MoO_3 and S powder respectively. MoO_3 was to be placed inside a quartz boat. A 300nmSiO_2/Si substrate is placed upon the open top of that boat, facing downwards towards the MoO_3 powder. Prior to this, the substrate was to be spin-coated with a layer of perylene-3,4,9,10- tetracarboxylic dianhydride (PTCDA), which is a seeding agent. The boat was inserted into a quartz tube, which in turn, was to be placed in the furnace. This boat was positioned in the tube such that it lies at the centre of the furnace where the heating is maximum. S powder was to be placed in another quartz boat at 7-8 cm upstream from the MoO_3 precursor. The S powder would be positioned inside the quartz tube, near the edge of the furnace where heating is less pronounced. Argon gas was to be passed through the quartz tube at all times during the experiment in order to maintain an inert environment.

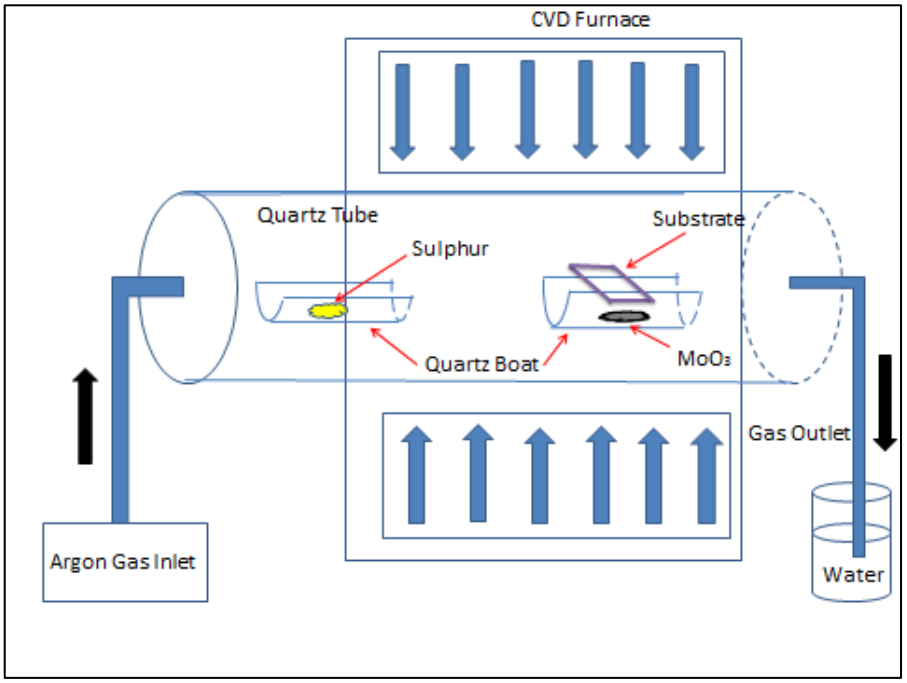

Figure 6.1. Schematic of CVD Furnace with substrate placement prior to sulphurisation.

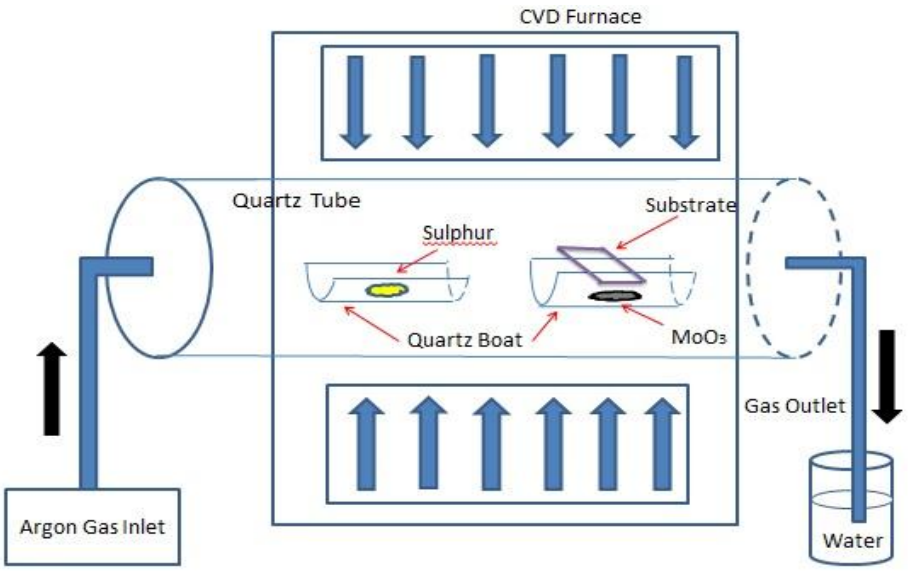

Figure 6.2. Schematic of CVD Furnace with substrate placement during and post sulphurisation.

Figure 6.3.Picture of CVD Furnace used for experimentation

In the early attempts, maintaining a ratio of 3:1 of MoO_3 and S powder by weight, different amounts of Sulphur powder and MoO_3 precursor were utilised. Initially, the tube would have to be shifted off the position along the upstream, during the warm up phase, in order to prevent the sulphur and MoO_3 powders from vaporising prematurely. When the growth temperature reaches around 650 ºC, the tube would be shifted back downstream to

its original position where the MoO_3 powder receives the maximum heating. The tube would be displaced further 3-4cm downstream off the usual placement for five minutes in order to facilitate sulphur vaporisation at this stage. The post-sulphurisation reaction would then be allowed to take place at its natural speed, thereby, continuing the Ar-gas flow at the same rate and lowering the temperature of the furnace to 200 ºC. The furnace takes around two hours to cool down to the room temperature. The tube is then removed from it and the substrate is extracted out of the boat with the help of a pair of tweezers and kept in a clean sample box. During this entire duration of the experiment, 150 sccm of constant Argon gas flow is maintained inside the tube, the gas inlet being that end of the tube containing the sulphur powder boat, while the other end of the tube is connected with a gas pipe that is dipped in a water- filled beaker. The trials with these conditions only yielded nominal nanoparticulate growth on certain random spots on the substrate surface. The deposition of MoS_2 nanoflakes was observed to be horizontal and looked quite hazy.

6.2 Successful Work

After the initial trials which resulted in futility, it was concluded that certain alterations need to be made in our adopted as those conditions for growth were far from idea. The observed nanoparticle growths and also, use of relatively clean substrates indicated that MoS_2 seeds were undergoing negligible nucleation and also, its vapour density was not sufficient enough for the formation of large crystal growth. This implied that the quantity, and in turn, weight ratio of the precursor and reactant needed to be changed. This could, however, be due to the application of low temperatures, which might not provide sufficient energy for formation of ordered crystal. Moreover, the faded deposition of the particles hinted that the reactants might not be available for enough time for reaction to be carried out on the substrate. One of the reasons for this could be the air flow with which the reactants might go downstream before undergoing the desired reaction.

In this later stage of work, increased amounts of the reactants were used. Various amounts of MoO_3 and sulphur powder are utilized, maintaining a ratio of 3:2 of MoO_3 and S powder by weight. Temperatures for growth were raised to 700 ºC to streamline the energy efficiency. However, it was decided not to increase the temperature in order to remain in the safe side , as the melting point of MoO_3 is known to be 795 ºC. Also the sulphur containing boat was placed at the extreme edge of the tube, so that there is no chance of vaporization of sulphur before the desired sulphurisation reaction takes place. The size of the SiO_2/Si substrates were

taken such that maximum area could be exposed to the reaction. These were some of the changes made in lieu of the renewed focus in guaranteeing the right conditions for growth were attained. Thus, the experimentation began by placing one such Si/SiO_2 substrate face down above the MoO_3 source. This could be done by utilising a quartz boat to hold the source and substrates, and also, using the lips of the boat as additional substrate support.

These experiments which were conducted using these new conditions yielded success.

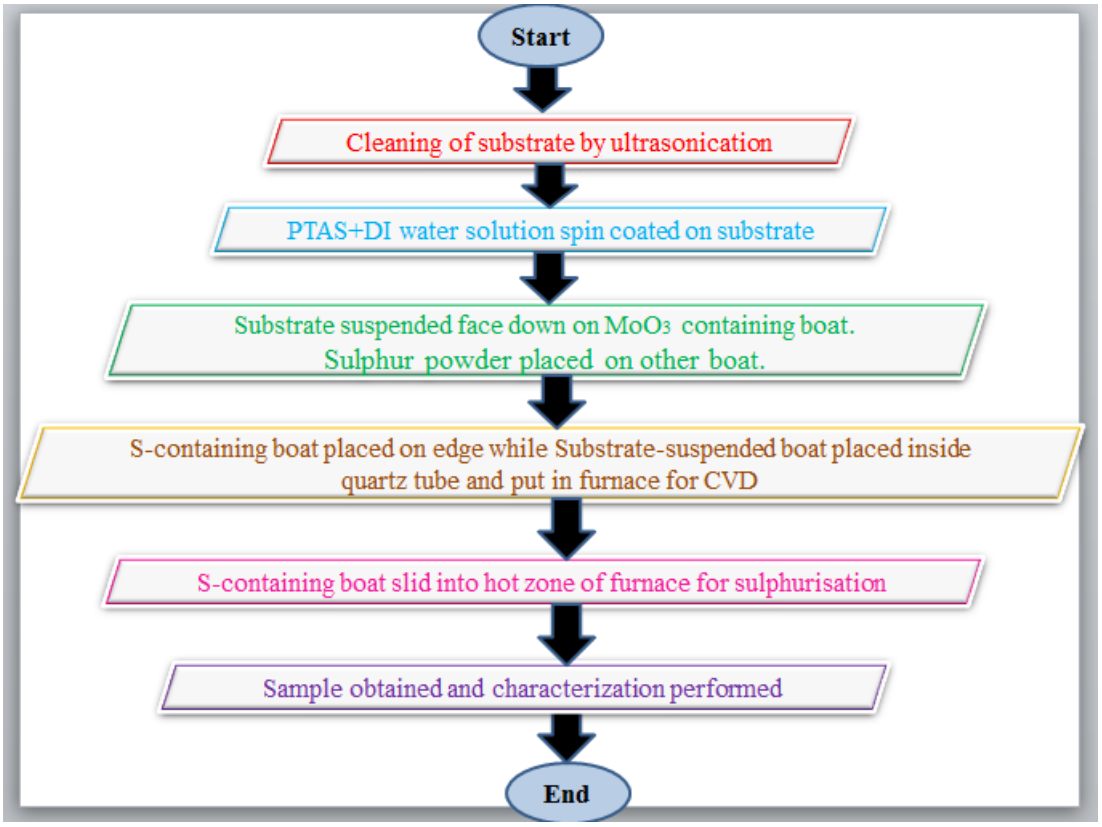

Figure 6.4. Flow Chart of the entire experimental process

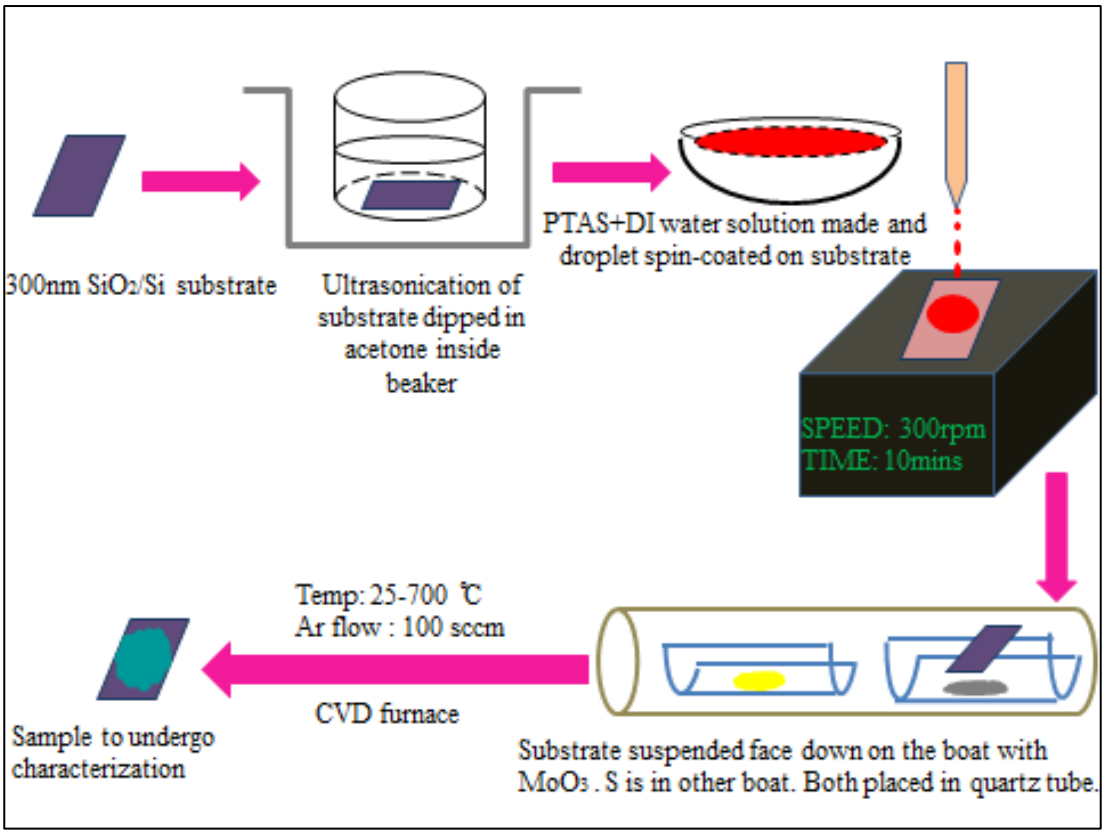

Figure 6.5. Block Diagram of the entire Experimental Process

Following are the specifications of the experiments in a detailed manner.

<u>Processing of substrate prior to CVD</u> :

1. Ultrasonication

A 300 nm SiO_2/Si substrate is taken as the substrate for growth of the MoS_2 monolayer. It is initially treated with acetone to remove any impurities adhered to its surfaces.

2. Spin Coating

A high solubility of PTCDA in deionized (DI) water enables a uniform distribution of the seeds on the hydrophilic substrate surfaces. Prior to the growth, a droplet of aqueous PTCDA solution, was spun on the SiO_2 surface of the substrate.

0.001g PTCDA in dissolved in 10mL DI water to form a homogeneous red solution. The substrate is then placed on a spin coater and dropwise the solution is put upon the SiO_2 surface and the apparatus is run at a low speed of 200-500 rpm for around 15-20 mins. The slow speed ensures unnecessary spilling of the droplets to the surrounding, and also, formation of a

uniform film of the seeding agent upon the substrate. It is then allowed to dry for around 10 mins. prior to CVD.

CVD Growth Procedure :

The MoO_3 powder (0.03 g) was placed in a ceramic boat and the seeding agent coated SiO_2/Si substrate is faced down and mounted on the top of boat. The boat is then placed in the hot zone of the furnace. During the synthesis of MoS_2 sheets, the reaction chamber was heated to 700°C in an argon environment of 150sccm.Upon attaining 700°C, the separate ceramic boat with sulfur powder (0.02 g) was slid from the extreme edge of the quartz tube, to be placed inside the furnace, next to the MoO_3 powder at a distance of 7-8 cm.

At such a high temperature, MoO_3 powder was reduced by the sulfur vapor to form volatile suboxide $MoO_{3-x.}$ These suboxide compounds diffused to the substrate and further reacted with sulfur vapor to grow MoS_2 films.

After 5 mins of Sulfur vapour exposure, the furnace temperature is gradually brought down to room temperature (27v°C) while the flow of Ar is maintained at 150 sccm. This cooling process takes around 2hrs approximately.

When taken out of the furnace, the substrate develops a bluish-green layer on areas exposed to sulfurization reaction, over the purple SiO_2 side of the substrate, indicating the formation of MoS_2 nanosheet.

Figure 6.6. Picture of the as-obtained sample.

Common Issues and Solutions:

At this point of work, a sleuth of commonly occurring issues did surface from time to time during the course of the project.

One simple issue was the risk of vaporization of MoO_3 precursor, prior to sulphurisation. This was easily solved by keeping the upper limit of the furnace temperature way below the melting point of the precursor.

Another large issue was the uneven nucleation of MoS_2 throughout the whole SiO_2/Si substrate. It is reported that MoS_2 was found to nucleate in and around large impurities or defects on the surface of substrate. Evenly separated nucleation is, thus, very difficult to obtain. There seems no simple solution for this persisting problem, apart from the use of seeding agents which was used in the experimental procedure of this project.

Another issue would be the inavailability of sulphur at the time of sulphurisation period. The sulphur tends to quickly melt and vaporize within the first few minutes of heating. This problem is resolved by placing the sulphur containing boat at the extreme edge of the quartz tube, so that it does not get heated until sulphurisation reaction takes place.
One more issue was the inaccuracy of the temperature displayed on the furnace panel. This is because the temperature of the furnace was not uniform throughout. The hottest temperature was reached at the centre of the furnace which was usually at least 100ºC above the displayed value. Hence, this issue was eliminated by using a thermocouple which could read the exact temperature of the furnace at its innermost core.

6.3 Discussions

One major point of probable source of error in this experiment would have to be the high temperatures used during the growth process. Temperatures expressed were purely based on the value shown on the furnace display. The temperature inside the furnace is not uniform . Also, the temperature would taper off by approximately 200ºC towards edges of the furnace. This systematically creates a substantial amount of discrepancy from the temperature displayed at the panel. This might be an issue, in case, if some other research groups with different setups having different specifications, wish to replicate the experiment.

Another probable source of error may stem up from the grain boundaries of MoS_2 as mentioned in the report by van der Zande et al[4]. The grain boundaries are found to have S or Mo terminations which result in the difference of electron densities and also, effective doping of the boundaries. This seriously could affect the photoluminescence data near the grain boundaries of the crystals of MoS_2. The grain boundaries may also affect the band gap by themselves, and may also lift off the surface of SiO_2/Si substrate which would strongly affect the photoluminescence data. Inspite of precautions taken in order to take data only at selected areas away from grain boundaries, however, photoluminescence peak values may still be affected by a systematic error, as found in literature, of about 26 meV upshift.

7 Results and Discussions

7.1 Atomic Force Microscopy:

XE100 model of AFM setup available at the Department of Applied Physics in Delhi Technological University was used to capture the AFM images of the as-produced samples.

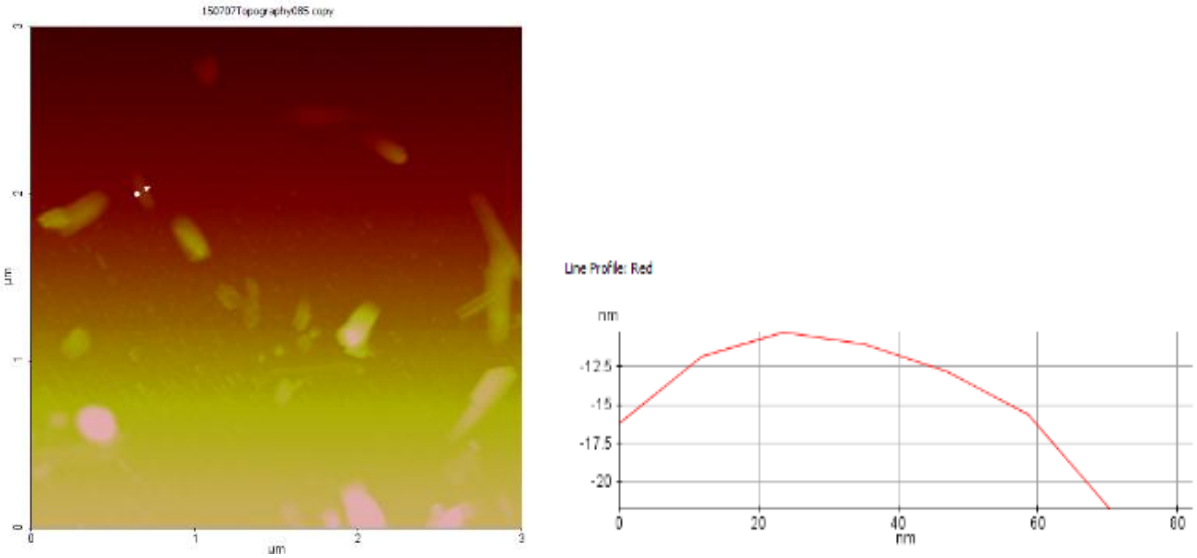

Figure 7.1. AFM image of single MoS_2 nanoparticulate growth indicating thickness.

The AFM images revealed that the deposition of as-grown MoS_2 monolayer is vertical and clean. In the above image, the thickness a single isolated MoS_2 flake is measured and found to be about 70 nm.

7.2 Scanning Electron Microscopy (SEM):

Hitachi S3700N model of SEM available at the Department of Applied Physics in Delhi Technological University was used to capture the SEM images of the as-produced samples. Some of the successful attempts have been illustrated below.

It shows the domain deposition evolution of as-grown MoS_2 on SiO_2/Si substrate. Notably, in the very first trial (Figure 7.1), hazy and faded random were deposited upon the substrate. Upon increasing the growth temperature to 700 ºC and reducing the Ar- flow to 100sccm, and subsequent, alteration in the weight ratios of the reactants, while keeping other growth parameters identical (Fig. 7.2 – 7.4), the deposition of the triangular MoS_2 flakes appeared distinct and formed small clusters with the increase in the number of such islands as well as the density of these MoS_2 flakes in those islands, as we proceed from trial no. 2 to trial no. 4. Such island growth hints at the catalytic action of the seeding agent, PTCDA, used during the experiment.

Trial no.1:

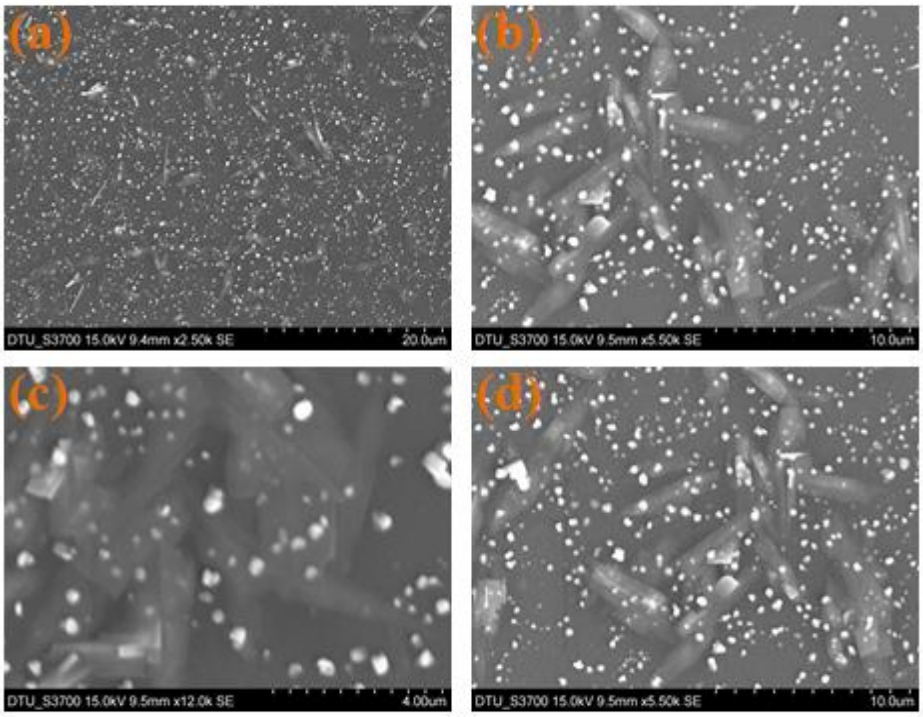

Figure 7.2. SEM image of nanoparticulate growth on the substrate.

Trial no.2:

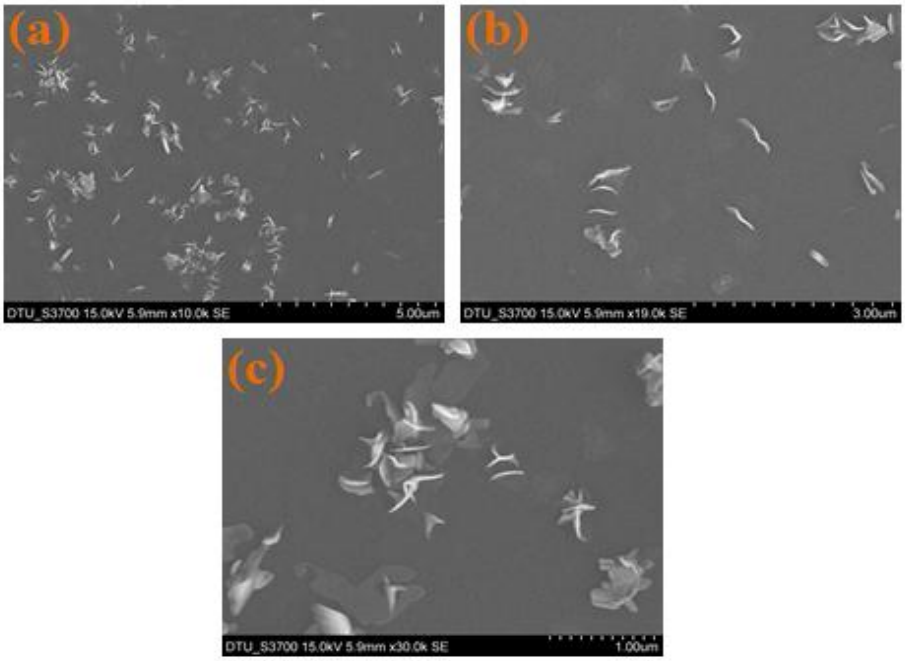

Figure 7.3. SEM image of island growth on the substrate.

Trial no.3:

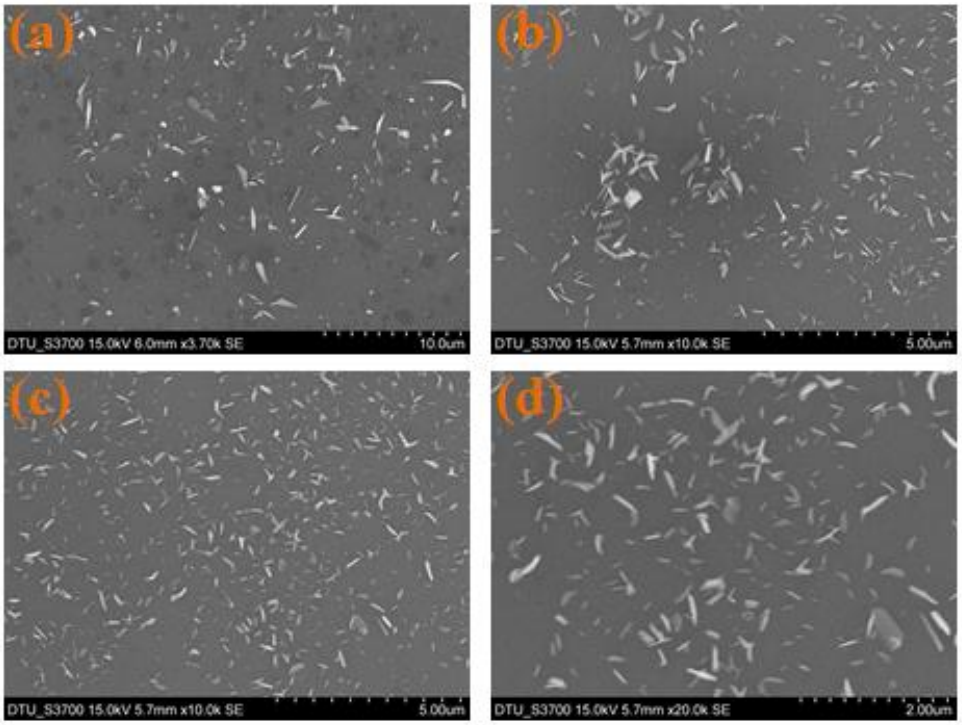

Figure 7.4. SEM image of scattered growth in a region on the substrate.

Trial no. 4:

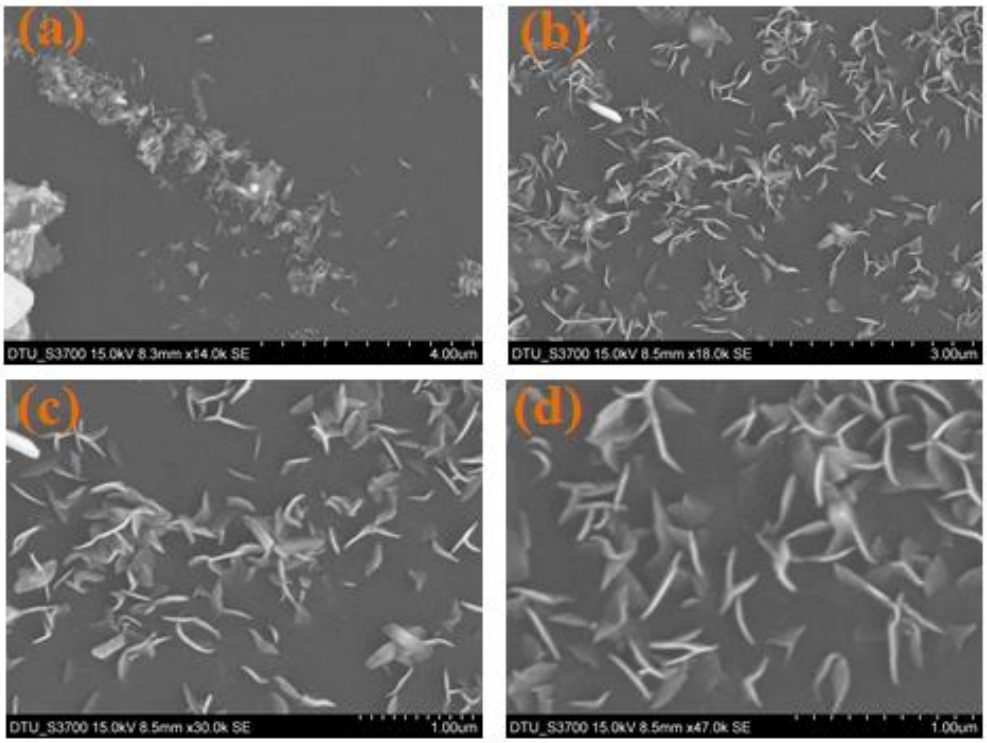

Figure 7.5. SEM image of continuous growth in a region on the substrate

7.3 Photoluminescence (PL) Spectrum:

To further verify the few layer thickness of this grown sample, an analysis of the photoluminescence spectra was needed, as shown in Figure 7.6 and 7.7. Florolog 3 Horiba model of PL setup available at the Department of Applied Physics in Delhi Technological University was used for the PL spectroscopy of the as-produced samples.

Sample no.2 :

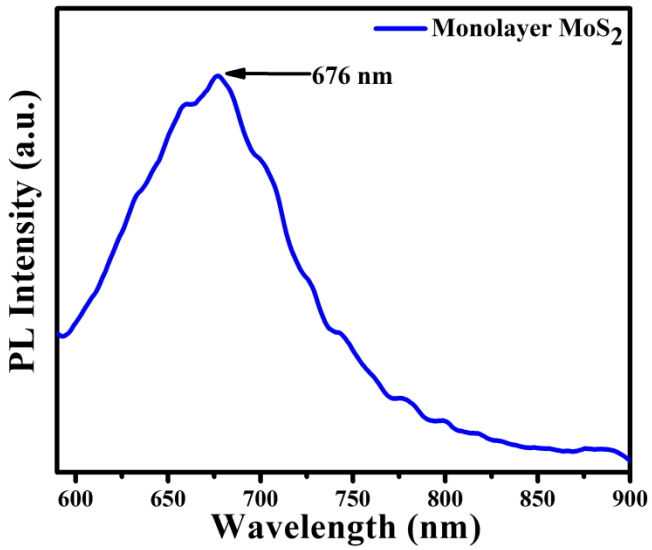

Figure 7.6. PL spectra of the MoS_2 sample no.2

Sample no.4 :

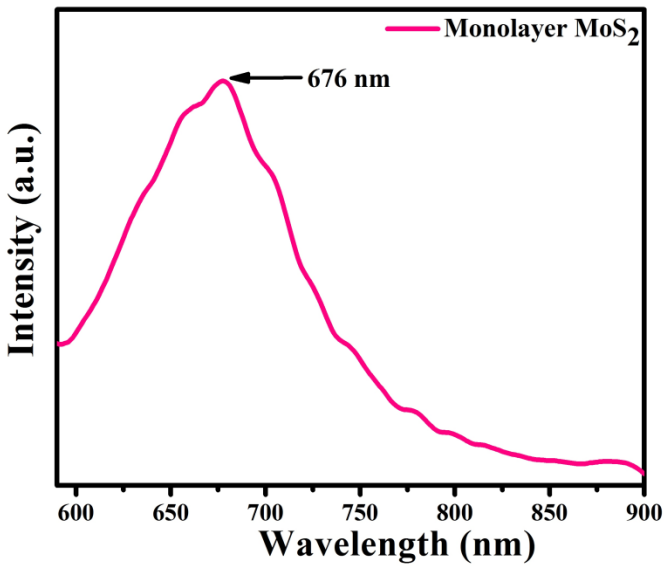

Figure 7.7. PL spectra of the MoS_2 sample no.4

A strong PL peak at 676 nm, with no shoulder peak was observed. Such single PL peak proves monolayer of MoS_2. In contrast, few-layer samples are reported to display multiple emission

peaks. This wavelength value of 676 nm. implies a bandgap of 1.83 eV which is much higher than the known MoS_2 bulk band gap of 1.29 eV. This is highly indicative of the growth being monolayer since such single strong PL peak as well as signature bandgap indicates the direct bandgap nature of the as-produced MoS_2 which occurs only in monolayer case. In all other cases, MoS_2 is known to be an indirect bandgap material.

7.4 UV-Vis Absorbance Spectrum:

Perkin Elmer Lambda 750 model of UV-Vis setup available at the Department of Applied Physics in Delhi Technological University was used was used for the UV-Vis spectroscopy of the as-produced samples.

Trial no. 2:

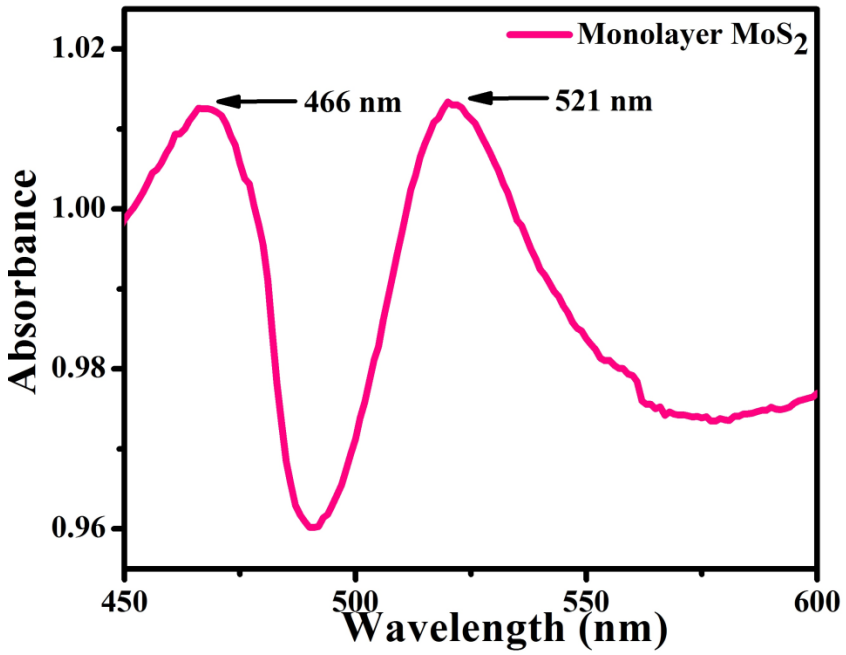

Figure 7.8. UV-Vis spectra of the MoS_2 sample no.2

Trial no. 4:

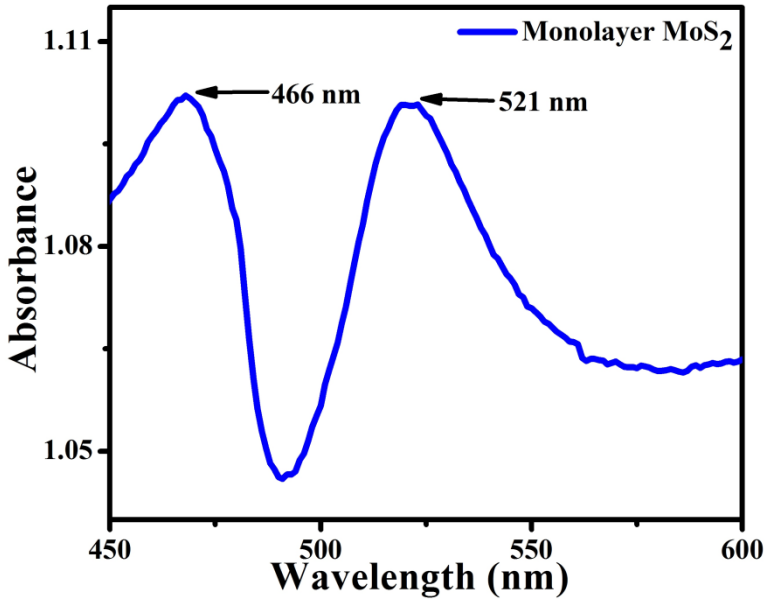

Figure 7.9. UV-Vis spectra of the MoS_2 sample no.4

Silicon dioxide was used as the reference to do away the effect of absorbance due to it upon the spectrum obtained. The spectrum shows two peaks at 466nm (2.66 eV) and 521 nm (2.37 eV) which can be assigned to the characteristics of MoS_2 nanosheet and correspond to the smallest direct transition. This demonstrates the high optical quality and uniformity of our monolayer MoS_2 over a large area. These peaks are associated to optical absorption by band-edge excitons, of monolayer MoS_2. The values of excitons showed a blue shift compared to the reported data for the bulk powder (748 nm (1.66 eV)). The blue shift is due to the quantum-size confinement.

8 Conclusion

The objective of this project was to design as well as implement a simple and inexpensive method for the growth of monolayer MoS_2 on SiO_2/Si substrate and to characterize it using standard available characterization techniques.

A chemical vapour deposition method was used as the synthesis route, within the means of the equipments available, in order to grow monolayer MoS_2. The conditions necessary for successful growth were thoroughly researched and experimentally fine tuned in order to achieve the desired reproducible growth of fairly large MoS_2 monolayer crystals. A chemical mixture of MoO_3 and S powder mixed in a weight ratio of 3:2 respectively was used. The sample was grown at 700 ºC for 5 minutes with 100 sccm of Ar gas flow.

Monolayer growth on SiO_2/Si substrate surface was confirmed and the results of the characterization techniques indicated successful growth of atleast film-like or monolayer of MoS_2 crystals.

8.1 Future Work

Although MoS_2 has been the centre of attraction amongst researchers for these last few years, however, a method for consistent and reproducible growth that is feasible for commercial purpose is still far off, as experienced during the course of this project. The recently released study report of *X. Ling et al*[30] depicts the steps in the right sequence as the MoS_2 growth progresses towards more even nucleation as well as lower temperatures requirement. Growths on alternative substrates are, however, still relatively understudied. Even though research is ongoing on construction of Graphene-MoS_2 heterostructures as photodetectors[39], much more can be done in order to explore the potential of MoS_2 heterostructures. In particular, monolayer crystalline MoS_2 growth on h-BN should be explored further, as h-BN is found to be superior 2D substrate[40]. Then the research could probably progress to transfer of graphene on to these MoS_2-BN heterostructures in order to form a 2D version of the traditional MOS transistor. Clearly, graphene would act as metal electrode, on the other hand, h-BN and MoS_2 would act as insulator and semiconductor respectively. This work could strongly pave the way to realization of 2D transistors in the near future.

9 References

1. X. Song, J. Hu and H. Zeng. Two-dimensional semiconductors: recent progress and future perspectives. *J. Mater. Chem. C*, 1, 2952-2969(2013).

2. K. F. Mak, C. Lee, J. Hone, J. Shan and T. F. Heinz. Atomically Thin MoS_2: A New Direct-Gap Semiconductor. *Physical Rev. Lett.*, 1050, 136805(2010).

3. C. Lee, H. Yan, L. E. Brus, T. F. Heinz, J. Hone and S. Ryu. Anomalous Lattice Vibrations of Single- and Few-Layer MoS_2. *ACS Nano,* 4, 5, 2695-2700(2010).

4. A. M. van der Zande, P. Y. Huang, D. A. Chenet, T. C. Berkelbach, Y. You, G. Lee, T. F. Heinz, D. R. Reichman, D. A. Muller and J. C. Hone. Grains and grain boundaries in highly crystalline monolayer molybdenum disulphide. *Nature Materials,* 12, 554-561(2013).

5. A. K. Geim and K. S. Novoselov. The Rise of Graphene. *Proc. Natl. Acad. Sci. U.S.A.* 102, 10451(2007).

6. D. Lembke and A. Kis. Breakdown of high-performance monolayer MoS_2 transistors. *ACS Nano.* 6, 10070(2012).

7. B. Radisavljevic, A. Radenovic, J. Brivio, V. Giacometti and A. Kis. Single-layer MoS_2 Transistors. *Nature Nano.* 6, 147-150(2011).

8. S. Bertolazzi, J. Brivio, A. Kis. Stretching and Breaking of Ultrathin MoS_2. *ACS Nano*. 5, 9703-9709(2011).

9. W. Zhu, T. Low, Y. Lee, H. Wang, D. B. Farrmer, J. Kong, F. Xia and P. Avouris. Ekectronic transport and device prospects of monolayer molybdenum disulphide grown by chemical vapor deposition. *Nature Communications.* 5, 3087(2014).

10. M. R. Laskar, L. Ma, S. Kannapan, P. S. Park, S. Krishnamoorthy, D. N. Nath, W. Lu, Y. Wu and S. Rajan. Large area single crystal (0001) oriented MoS_2. *Appl. Phys. Lett.* 102, 252108(2013).

11. Q. Li, J. T. Newberg, E. C. Walter, J. C. Hemminger and R. M. Penner. Polycrystalline Molybdenum Disulfide (2H- MoS_2) Nano- and Microribbons by Electrochemical/Chemical Synthesis. *Nano Letters.* 4, 277-281(2004).

12. K. Liu, W. Zhang, Y. Lee, Y. Lin, M. Chang, C. Su, C. Chang, H. Li, Y. Shi, H. Zhang and C. Lai, L. Li. Growth of Large-Area and Highly Crystalline MoS_2 Thin Layers on

Insulating Substrates. *Nano Lett.* 12, 1538-1544(2012).

13. C. Gong, C. Huang, J. Miller, L. Cheng, Y. Hao, D. Coben, J. Kim, R. S. Ruoff, R. M. Wallace, K. Cho, X. Xu and Y. J. Chabal. Metal Contacts on Physical Vapor Deposited Monolayer MoS_2. *ACS Nano.* 7, 11350-11357(2013).

14. Y. Lee, X. Zhang, W. Zhang, M. Chang, C. Lin, K. Chang, Y. Yu, J. T. Wang, C. Chang, L. Li and T. Lin. Synthesis of Large-Area MoS_2 Atomic Layers with Chemical Vapor Deposition. *Adv. Mater.* 24, 2320-2325(2012).

15. Y. Lee, L. Yu, H. Wang, W. Fang, X. Ling, Y. Shi, C. Lin, J. Huang, M. Chang, C. Chang, M. Dresselhaus, T. Palacios, L. Li and J. Kong. Synthesis and Transfer of Single-Layer Transition Metal Disulfides on Diverse Surfaces. *Nano Lett.*13, 1852-1857(2013).

16. S. Najmaei, Z. Liu, W. Zhou, X. Zou, G. Shi, J. Odrpbp, P. M. Ajayan and J. Lou. Vapour phase growth and grain boundary structure of molybdenum disulphide atomic layers. *Nature Materials,* 12, 754-759(2013).

17. X. Wang, H. Feng, Y. Wu and L. Jiao. Controlled Synthesis of Highly Crystalline MoS_2 Flakes by Chemical Vapor Deposition. *J. Am. Chem. Soc.* 135, 5304-5307(2013).

18. Y. Cheng, K. Yao, Y. Yang, L. Li, Y. Yao, Q. Wang, X. Zhang, Y. Han and U. Schwingenschlögl. Van der Waals epitaxial growth of MoS_2 on SiO_2/Si by chemical vapor deposition. *RSC Advances,* 3, 17287-17293(2013).

19. Y. Shi, W. Zhou, A. Lu, W. Fang, Y. Lee, A. L. Hsu, S. M. Kim, K. K. Kim, H. Y. Yang, L. Li, J. Idrobo and J. Kong. van der Waals Epitaxy of MoS_2 Layers Using Graphene As Growth Templates. *Nano lett.* 12, 2784-2791 (2012).

20. Y. Yu, C. Li, Y. Liu, L. Su, Y. Zhang and L. Cao. Controlled Scalable Synthesis of Uniform, High-Quality Monolayer and Few-layer MoS_2 Films. *Scientific Reports,* 3, 1866(2013).

21. Y. Zhan, Z. Liu, S. Najmaei, P. M. Ajayan and J. Lou. Large-Area Vapor-Phase Growth and Characterization of MoS_2 Atomic Layers on a SiO_2 Substrate. *small,* 8, No.7, 966-971(2012).

22. P. Tonndorf, R. Schmidt, P. Bottger, X. Zhang, J. Borner, A. Liebig, M. Albrecht, C. Kloc, O. Gordan, D. R. T. Zahn, S. M. de Vasconcellos and R. Batschitsch. Photoluminescence emission and Raman response of monolayer MoS_2, MoSe2 andWSe2. *Optics express*, 21(4) 4908-4916(2013).

23. A. RamasubRamaniam, D. Naveh and E. Towe. Tunable band gaps in bilayer transition-metal dichalcogenides. *Physical Review B.* 84, 205325(2011).

24. A. A. Bolzan, B. J. Kennedy and C.J. Howard. Neutron powder diffraction study of molybdenum and tungsten dioxides. *Austr. J. Chem.*, 48, 1473(1995).

25. A. Splendiani, L. Sun, Y. Zhang, T. Li, J. Kim, C. Chim, G. Galli and F. Wang. Emerging Photoluminescence in Monolayer MoS_2. *Nano. Lett.*10, 1271-1275(2010).

26. J. Carlsson, P. M. Martin Handbook of Deposition Technologies for Films and Coatings: Science, Applications and Technology. *Elsevier Inc*(2010).

27. A. C. Jones, M. L. Hitchman. Chemical Vapor Deposition: Precursors, Processes and Applications. *Royal Society of Chemistry*(2009).

28. Z. Matusinovic, R. Shukla, E. Manias, C. G. Hogshead, C. A. Willkie. Polystyrene/molybdenum disulfide and poly(methyl methacrylate)/molybdenum disulfide nanocomposites with enhanced thermal stability. *Elsevier*. 97, 2481-2486(2012).

29. S. K. Das, R. Mallavajula, N. Jayaprakash and L. A. Archer. Self-assembled MoS_2-carbon nanostructures: influence of nanostructuring and carbon on lithium battery performance. *J. Mater. Chem.* 22, 12988-12992(2012).

30. X. Ling, Y. Lee, Y. Lin, W. Fang, L. Yu, M. S. Dresselhaus and J. Kong. Role of the seeding Promoter in MoS2 Growth by Chemical Vapor Deposition. *Nano. Lett.* 14, 464-472(2014).

31. N. H. Fletcher. Size Effect in Heterogeneous Nucleation. *J. Chem. Phys.* 29, 572-576(1958).

32. D. J. Turnbull. Kinetics of Heterogeneous nucleation. *J. Chem. Phys.* 18, 198-203(1950).

33. X. Lu, M. I. B. Utama, J. Zhang, Y. Zhao and Q. Xiong. Layer-by-layer thinning of MoS_2 by thermal annealing. *Nanoscale.* 5, 8904(2013).

34. A. Molina-Sanchez, L. Wirtz. Phonons in single-layer and few-layer MoS_2 and WS_2 *Phys. Rev. B.* 84, 155413(2011).

35. J. Aizenberg, A. J. Black, G. M. Whitesides. Control of crystal nucleation by patterened self-assembled monolayers. *Nature.* 398, 495-498(1999).

36. Q. Ji, Y. Zhang, T. Gao, Y. Zhang, D. Ma, M. Liu, Y. Chen, X. Qiao, P. Tan, M. Kan, J. Feng, Q. Sun and Z. Liu. Epitaxial Monolayer MoS_2 on Mica with Novel Photoluminescence. *Nano. Lett.* 13, 3870-3877(2013).

37. M. Chhowalla, H. S. Shin, G. Eda, L. Li, K. P. Loh and H. Zhang. The chemistry of two-dimensional layered transition metal dichalcogenide nanosheets. *Nature Chemistry*. 5, 263-275(2013).

38. H. Li, G. Lu, Z. Yin, Q. He, H. Li, Q. Zhang and H. Zhang. Optical Identification of Single- and Few-Layer MoS_2 sheets. *Small*, 8, 682-686(2012).

39. W. Zhang, C. Chuu, J. Huang, C. Chen, M. Tsai, Y. Chang, C. Liang, Y. Chen, J. He, M. Chou and L. Li. Ultrahigh-Gain Photodetectors Based on Atomically Thin Graphene-MoS_2 Heterostructures. *Scientific Reports.* 4, 3826(2014).

40. C. R. Dean, A. F. Young, I. Meric, C. Lee, L. Wang, S. Sorgenfrei, K. Watanabe, T. Taniguchi, P. Kim, K. L. Shepard and J. Hone. Boron nitride substrates for high-quality graphene electronics. *Nature Nanotechnology.* 5, 722-726(2010).

41. Lin Ma, Wei-Xiang Chen, Li-Mei Xu, Xiao-Ping Zhou, Bei Jin. One-pot hydrothermal synthesis of MoS_2 nanosheets/C hybrid microspheres. Ceramics International 38 (2012) 229–234

42. Lijuan Ye, Haiyan Xu , Dingke Zhang, Shijian Chen. Materials Research Bulletin 55 (2014) 221–228

43. Yufei Zhao, Yuxia Zhang, Zhiyu Yang, Yiming Yan and Kening Sun. Synthesis of MoS_2 and MoO_2 for their applications in H_2 generation and lithium ion batteries: a review. Sci. Technol. Adv. Mater. **14** (2013) 043501

44. Yifei Yu, Chun Li, Yi Liu, Liqin Su,Yong Zhang, Linyou Cao. Controlled Scalable Synthesis of Uniform, High-Quality Monolayer and Few-layer MoS_2 Films. *Scientific Reports*3, Article number:1866doi:10.1038/srep01866

45. Kiran Kumar Amara, Leiqiang Chu,Rajeev Kumar,Minglin Toh,and Goki Eda. Wet chemical thinning of molybdenum disulfide down to its monolayer. APL Materials **2**, 092509 (2014); doi: 10.1063/1.4893962

46. Xi Ling, Yi-Hsien Lee, Yuxuan Lin, Wenjing Fang, Lili Yu,Mildred S. Dresselhaus, and Jing Kong. Role of the Seeding Promoter in MoS_2 Growth by Chemical Vapor Deposition. *Nano Lett. 2014, 14, 464−472.*

47. Sohail Ahmad, Sugata Mukherjee. Graphene, 2014, 3, 52-59

48. A.K.M. Newaz, D.Prasai, J.I.Ziegler, D.Caudel, S.Robinson, R.F.HaglundJr., K.I.Bolotin . Solid State Communications 155 (2013) 49–52

49. Wu Zhou, Xiaolong Zou, Sina Najmaei, Zheng Liu, Yumeng Shi, Jing Kong, Jun Lou, Pulickel M. Ajayan, Boris I. Yakobson, and Juan-Carlos Idrobo. . Nano Lett. 2013, 13, 2615−2622

50. Nanjundan Ashok Kumar, Mushtaq Ahmad Dar, Rukhsana Gul and Jong-Beom Baek. Materials Today Volume 18, Number 5 June 2015

51. Wenjuan Zhu, Tony Low, Yi-Hsien Lee, Han Wang, Damon B. Farmer, Jing Kong, Fengnian Xia & Phaedon Avouris. NATURE COMMUNICATIONS | DOI: 10.1038/ncomms4087

52. Arend M. Van der Zande, Pinshane Y. Huang,Daniel A.Chenet,TimothyC. Berkelbach,Youmeng You5, Gwan---Hyoung Lee, Tony F.Heinz1,David R.Reichman,DavidA.Muller3,James C.Hone. Grains And grain boundaries in highly crystalline monolayer molybdenum disulfide

53. R. Ansari, S. Malakpour, M. Faghihnasiri, and S. Ajori. Journal of Nanotechnology in Engineering and Medicine AUGUST 2013, Vol. 4 / 034501-1

54. Jia Zhang, Jia Mei Soon,Kian Ping Loh, Jianhua Yin, Jun Ding,Michael B. Sullivian,and Ping Wu. Nano Lett., Vol. 7, No. 8, 2007

55. Kangho Lee , Hye-Young Kim , Mustafa Lotya , Jonathan N. Coleman , Gyu-Tae Kim ,and Georg S. Duesberg. *Adv. Mater.* 2011, *23*, 4178–4182

56. EhrenM.Mannebach, Karel-AlexanderN.Duerloo, Lenson A. Pellouchoud,Meng-Ju Sher, SangheeNah,Yi-Hong Kuo, Yifei Yu, Ann F. Marshall,Linyou Cao,Evan J. Reed,and Aaron M. Lindenberg. American Chemical Society, VOL. 8,NO. 10 ,10734–10742, 2014.